



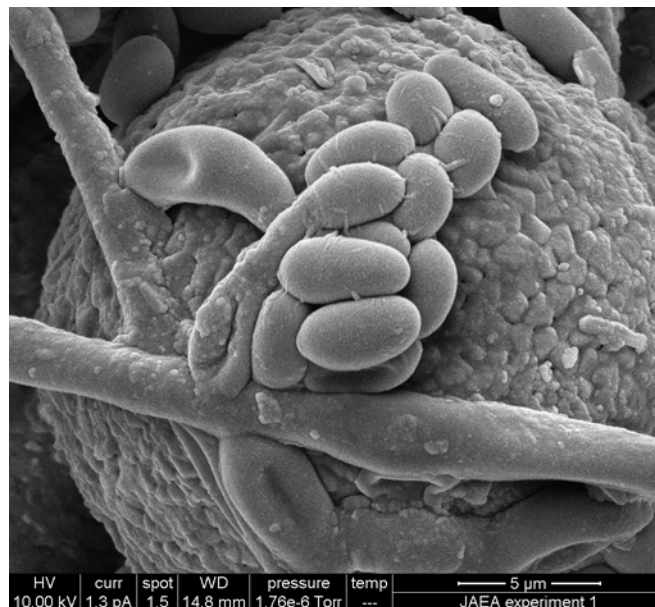
**British  
Geological Survey**

NATURAL ENVIRONMENT RESEARCH COUNCIL

# Microbiological effects on transport processes (BioTran) Data production from column experiments for use in microbial models (April 2009 - March 2010)

Radioactive Waste Programme

Open Report OR/10/067





BRITISH GEOLOGICAL SURVEY

RADIOACTIVE WASTE PROGRAMME

OPEN REPORT OR/10/067

# Microbiological effects on transport processes (BioTran) Data production from column experiments for use in microbial models (April 2009 - March 2010)

## *Keywords*

Geomicrobiology,  
biofilms, columns, fracture  
surfaces, Horonobe, mudstone.

H Harrison, J M West, A E Milodowski, K Bateman, P Coombs, J  
Harrington, S Holyoake, A Lacinska, G Turner and D Wagner.

## *Front cover*

CryoSEM SEI image showing  
detail of the clusters rod-like  
cells associated with biofilaments  
resting on fresh framboidal pyrite

## *Contributor/editor*

R P Shaw

## *Bibliographical reference*

H HARRISON, J M WEST, A E  
MILODOWSKI, K BATEMAN, P  
COOMBS, J HARRINGTON, S  
HOLYOAKE, A LACINSKA, G  
TURNER AND D WAGNER.. 2010.  
*British Geological Survey Open  
Report, OR/10/067. 59pp.*

Copyright in materials derived  
from the British Geological  
Survey's work is owned by the  
Natural Environment Research  
Council (NERC) and/or the  
authority that commissioned the  
work. You may not copy or adapt  
this publication without first  
obtaining permission. Contact the  
BGS Intellectual Property Rights  
Section, British Geological  
Survey, Keyworth,  
e-mail [ipr@bgs.ac.uk](mailto:ipr@bgs.ac.uk). You may  
quote extracts of a reasonable  
length without prior permission,  
provided a full acknowledgement  
is given of the source of the  
extract.

Maps and diagrams in this book  
use topography based on  
Ordnance Survey mapping.

## BRITISH GEOLOGICAL SURVEY

The full range of our publications is available from BGS shops at Nottingham, Edinburgh, London and Cardiff (Welsh publications only) see contact details below or shop online at [www.geologyshop.com](http://www.geologyshop.com)

The London Information Office also maintains a reference collection of BGS publications, including maps, for consultation.

We publish an annual catalogue of our maps and other publications; this catalogue is available online or from any of the BGS shops.

*The British Geological Survey carries out the geological survey of Great Britain and Northern Ireland (the latter as an agency service for the government of Northern Ireland), and of the surrounding continental shelf, as well as basic research projects. It also undertakes programmes of technical aid in geology in developing countries.*

*The British Geological Survey is a component body of the Natural Environment Research Council.*

*British Geological Survey offices*

### **BGS Central Enquiries Desk**

Tel 0115 936 3143 Fax 0115 936 3276  
email [enquiries@bgs.ac.uk](mailto:enquiries@bgs.ac.uk)

### **Kingsley Dunham Centre, Keyworth, Nottingham NG12 5GG**

Tel 0115 936 3241 Fax 0115 936 3488  
email [sales@bgs.ac.uk](mailto:sales@bgs.ac.uk)

### **Murchison House, West Mains Road, Edinburgh EH9 3LA**

Tel 0131 667 1000 Fax 0131 668 2683  
email [scotsales@bgs.ac.uk](mailto:scotsales@bgs.ac.uk)

### **Natural History Museum, Cromwell Road, London SW7 5BD**

Tel 020 7589 4090 Fax 020 7584 8270  
Tel 020 7942 5344/45 email [bgs\\_london@bgs.ac.uk](mailto:bgs_london@bgs.ac.uk)

### **Columbus House, Greenmeadow Springs, Tongwynlais, Cardiff CF15 7NE**

Tel 029 2052 1962 Fax 029 2052 1963

### **Maclean Building, Crowmarsh Gifford, Wallingford OX10 8BB**

Tel 01491 838800 Fax 01491 692345

### **Geological Survey of Northern Ireland, Colby House, Stranmillis Court, Belfast BT9 5BF**

Tel 028 9038 8462 Fax 028 9038 8461

[www.bgs.ac.uk/gsni/](http://www.bgs.ac.uk/gsni/)

### *Parent Body*

### **Natural Environment Research Council, Polaris House, North Star Avenue, Swindon SN2 1EU**

Tel 01793 411500 Fax 01793 411501  
[www.nerc.ac.uk](http://www.nerc.ac.uk)

Website [www.bgs.ac.uk](http://www.bgs.ac.uk)

Shop online at [www.geologyshop.com](http://www.geologyshop.com)

# Foreword

This work was undertaken for the BGS BioTran project and for JAEA, Japan.

# Acknowledgements

We acknowledge the BGS, the JAEA and the Ministry of Economy, Trade and Industry of Japan (METI). We thank Ms Mai Kawagoe (Mitsubishi Corporation) for her assistance with the smooth running of the project and the BGS Analytical Chemistry Sections for their able assistance.

# Contents

<b>Foreword</b> .....	<b>i</b>
<b>Acknowledgements</b> .....	<b>i</b>
<b>Contents</b> .....	<b>i</b>
<b>Summary</b> .....	<b>vi</b>
<b>1 Introduction</b> .....	<b>1</b>
<b>2 Column Experiments</b> .....	<b>1</b>
2.1 Preparation of fluids .....	2
2.2 Preparation of intact core material .....	2
2.3 Bacterial culture .....	2
2.4 Analytical Techniques .....	3
2.5 Experimental design .....	8
2.6 Assembly of Column experiments .....	9
2.7 Decommissioning of Column experiments .....	12
<b>3 Results – Physical Measurements</b> .....	<b>14</b>
3.1 Biotic Core .....	14
3.2 Abiotic Core .....	15
<b>4 Results – Fluids</b> .....	<b>16</b>
4.1 Microbiology .....	16
4.2 Fluid Chemistry .....	17
<b>5 Results – Solid materials</b> .....	<b>17</b>
5.1 Whole rock mineralogical analysis .....	17
5.2 Clay mineral observations .....	18
5.3 BET surface area analysis .....	18

5.4	Optical and scanning electron microscopy observations.....	19
<b>6</b>	<b>Discussion.....</b>	<b>35</b>
<b>7</b>	<b>Conclusions .....</b>	<b>37</b>
<b>8</b>	<b>Recommendations .....</b>	<b>38</b>
<b>Appendix 1</b>	<b>Groundwater composition .....</b>	<b>1</b>
<b>Appendix 2</b>	<b>Fluid chemistry .....</b>	<b>2</b>
<b>Appendix 3</b>	<b>X-ray diffraction traces.....</b>	<b>5</b>
<b>References</b>	<b>.....</b>	<b>10</b>

## FIGURES

Figure 1	Schematic of column design.....	8
Figure 2	Schematic of pressure vessel with column containing rock core. ....	9
Figure 3	Core prior to emplacement in column. (Biotic experiment).....	9
Figure 4	Use of heat gun to shrink tubing around cut core. (Biotic experiment).....	10
Figure 5	Close up of tubing around core showing fracture (Biotic experiment) .....	10
Figure 6	Completed column prior to emplacement in pressure vessel. Note formation of lateral fracture which occurred during preparation (Biotic experiment).....	11
Figure 7	Assembly prior to inversion and placement into pressure vessel (Biotic experiment)...	11
Figure 8	Fully completed apparatus showing the attached pump assembly (Biotic experiment). 12	
Figure 9	Assembly after removal from pressure vessel (Biotic experiment).....	12
Figure 10	Further view of assembly after removal from pressure vessel (Biotic experiment).....	13
Figure 11	Column after removal from platen. Arrow shows direction of fluid flow during the experiment (Biotic experiment).....	13
Figure 12	Removal of second platen (Biotic experiment) .....	13
Figure 13	Biotic experiment: injection and confining pressure data plotted against experiment duration in days .....	14
Figure 14	Abiotic experiment: injection and confining pressure data plotted against experiment duration in days .....	15

## PLATES

Plate 1	BSEM image (from VPSEM) showing the morphology and mineralogy of the fracture surface in the starting material. Angular fragments of microporous siliceous diatoms make up a large part of the sample. Fragments of cylindrical siliceous sponge spicules, together with angular detrital quartz silt grains and irregular silt-grade aggregates of detrital illitic clay can also be seen. (Starting material). LEO 435VP SEM instrument. ....	19
---------	---	----

Plate 2 BSEM image (from VPSEM) showing relatively large and complete cylindrical siliceous diatom skeleton with a compact groundmass of detrital clay, amorphous siliceous material and finer diatomaceous detritus. Fine bright grains of disseminated pyrite, with octahedral crystal forms, can be seen disseminated in the matrix. (Starting material). .....	20
Plate 3 BSEM image (from VPSEM) showing framboidal aggregates of fine grained pyrite forming a discrete “pod” within the siliceous diatomaceous matrix. (Starting material). LEO 435VP SEM instrument.....	20
Plate 4 BSEM image (from VPSEM) showing fine “ridge-and-furrow” ornamentation (with steeper “scarp” and gentler “tail” slopes) forming an interconnected network of sub-parallel to anastomosing fine channels along the fracture plane. (Starting material). LEO 435VP SEM instrument.....	21
Plate 5 BSEM image (from VPSEM) showing fine “ridge-and-furrow” ornamentation (with steeper “scarp” and gentler “tail” slopes) forming an interconnected network of sub-parallel to anastomosing fine channels along the fracture plane. (Starting material). LEO 435VP SEM instrument.....	22
Plate 6 BSEM image (from VPSEM) showing fine silt particles accumulated within the channels formed by the “ridge-and-furrow” lineaments on the fracture surface. (Starting material). LEO 435VP SEM instrument.....	22
Plate 7 BSEM image (from VPSEM) showing network of fine organic filaments (possibly fungal hyphae) growing across the fracture surface, following and penetrating along the interconnected network of sub-parallel to anastomosing fine slickenside channels in the fracture plane. (Starting material). LEO 435VP SEM instrument. ....	23
Plate 8 BSEM image (from VPSEM) showing detail of the fine organic filaments coating the fracture plane. (Starting material). LEO 435VP SEM instrument. ....	23
Plate 9 Binocular microscope photomicrograph showing annulus channel in the outer wall of the core plug where a fragment of the opposing fracture wall has fallen away. Post-experimental material. (Biotic experiment).....	24
Plate 10 Binocular microscope photomicrograph showing surface of the annulus channel in the outer wall of the core plug where a fragment of the opposing fracture wall has fallen away. Loose mineral fines are bonded to the surface by a gelatinous organic film. Post-experimental material. (Biotic experiment).....	25
Plate 11 Binocular microscope photomicrograph of the fracture surface showing the “ridge-and-furrow” features formed by slickensiding, and representing a network of fine microporous channels along the plane of the fracture. Post-experimental material. (Biotic experiment). .	25
Plate 12 CryoSEM SEI image (high vacuum cryoSEM, FEI ESEM instrument) of the fracture surface revealing a network of organic biofilaments following “ridges-and-furrows in the fracture surface. Post-experimental material. (Biotic experiment). High vacuum cryoSEM, uncoated sample, FEI ESEM instrument.....	26
Plate 13 CryoSEM SEI image of the fracture surface showing clusters of cellular structures associated with biofilaments and showing that some biofilaments comprise strings of rod-like cells. Post-experimental material. (Biotic experiment). High vacuum cryoSEM, uncoated sample, FEI ESEM instrument.....	27
Plate 14 CryoSEM SEI image of the fracture surface showing isolated rod-like cells associated with biofilaments that appear to comprise strings of connected rod-like cells that appear to be coated and obscured within the filament by an organic biofilm forming a sheath to the filament. Post-experimental material. (Biotic experiment). High vacuum cryoSEM, gold-coated sample, FEI ESEM instrument.....	27

Plate 15 CryoSEM SEI image of the fracture surface showing clusters of rod-like cells associated with biofilaments that appear to comprise strings of connected rod-like cells that appear to be coated and obscured within the filament by an organic biofilm forming a sheath to the filament. Post-experimental material. (Biotic experiment). High vacuum cryoSEM, gold-coated sample, FEI ESEM instrument.....	28
Plate 16 CryoSEM SEI image of the fracture surface showing detail of clusters of rod-like cells associated with biofilaments. Post-experimental material (Biotic Experiment). High vacuum cryoSEM, uncoated sample, FEI ESEM instrument. ....	28
Plate 17 CryoSEM SEI image showing clusters rod-like cells associated with biofilaments resting on fresh framboidal pyrite. Post-experimental material. (Biotic experiment). High vacuum cryoSEM, gold coated sample, FEI ESEM instrument.....	29
Plate 18 CryoSEM SEI image showing detail of the clusters rod-like cells associated with biofilaments resting on fresh framboidal pyrite. Fine pili structures can be seen on the rod-like cells that may function to bind the cell to mineral surfaces and adjacent cells. The pyrite appears to be unaffected by oxidation but the biofilaments can be seen to have etched into and are now embedded in the pyrite surface. Post-experimental material. (Biotic experiment). High vacuum cryoSEM, gold coated sample, FEI ESEM instrument. ....	29
Plate 19 CryoSEM SEI image showing a biofilaments that can be seen to have etched into and is now embedded in the siliceous sedimentary rock surface. Post-experimental material (Biotic experiment). High vacuum cryoSEM, gold-coated sample, FEI ESEM instrument.....	30
Plate 20 Macrograph of the reacted core plug directly after recovery from the a(Biotic experiment). A steep (70-80° dipping) fracture can be clearly seen. The trace of a second lower-angle (c.30° dipping) fracture can be seen as a dark trace on the core wall. The core has a small channel along the intersection between the fracture plane and the core cylinder wall, formed where a small amount of one fracture wall has broken away. Direction of fluid flow is shown. (Abiotic control experiment). ....	31
Plate 21 Binocular microscope photomicrograph showing detail of the annulus channel in the outer wall of the core plug where a second lower angle fracture intersects with the principal steeply inclined fracture. The fracture wall at the intersection of these fractures has partially brecciated and fragments of this broken wallrock have fallen away during core plug preparation to leave this channel along part of the core wall. Fracture porosity exists between the fragmented material within the steep fracture. Post-experimental material. (Abiotic control experiment).....	31
Plate 22 Binocular microscope photomicrograph showing detail of the surface of the main steep fracture. The fracture surface exhibits a series of ridges and furrows where the surface is intersected by lower angle hairline microfractures. These asperities in the fracture surface probably produce channelled flow. Post-experimental material. (Abiotic experiment).....	32
Plate 23 ESEM SEI image showing typical rough fracture wallrock surface devoid of any microbiological features. Post-experimental material. (Abiotic experiment). ESEM uncoated sample, FEI ESEM instrument. ....	33
Plate 24 BSEM image of fracture wallrock showing fabric dominated by well-preserved silica diatom structures material and fine grained silica matrix comprised of finely comminuted diatomaceous debris. Well preserved diagenetic pyrite can be seen as framboidal aggregates and as fine pyrite locally replacing the diatom structures. Post-experimental material. (Abiotic experiment). VPSEM uncoated sample, LEO 435VP SEM instrument.....	33
Plate 25 ESEM SEI image showing fracture surface composed of fine fragmented biogenic silica derived from sponge spicules and siliceous diatom skeletons. Post-experimental material. (Abiotic experiment). ESEM uncoated sample, FEI ESEM instrument. ....	34

Plate 26 ESEM SEI image showing well-preserved framboidal aggregates of authigenic pyrite exposed in the fracture surface. Post-experimental material. (Abiotic experiment). ESEM uncoated sample, FEI ESEM instrument.....	34
Plate 27 ESEM SEI image showing well-preserved octahedral microcrystals of authigenic pyrite exposed in the fracture surface. The matrix of the rock comprises abundant fine silt-grade silica diatom detritus. Post-experimental material. (Abiotic experiment). ESEM uncoated sample, FEI ESEM instrument. ....	35

## **TABLES**

Table 1 Composition of synthetic groundwater .....	2
Table 2 Mean total counts of bacteria by epifluorescence microscopy (Biotic experiment).....	16
Table 3 Summary of quantitative whole-rock XRD analyses.....	17
Table 4 Summary of BET/nitrogen surface area analyses .....	18

## Summary

The BioTran project was initiated to examine the effects of microbes on sub-surface transport processes, especially in the context of geological disposal of radioactive waste. Early work focussed on hard rock environments using dioritic material from the Äspö Underground Research Laboratory (URL). In 2008-2009, the scope of Biotran broadened to encompass batch experiments on mudstones, host rocks relevant to radioactive waste management in Japan. The 2009-2010 BioTran work programme furthers this work by using column experiments to investigate the effects of microbes on fractured mudstone. This work was undertaken on behalf of the Japanese Atomic Energy Authority (JAEA) and part-funded by the Ministry of Economy, Trade and Industry of Japan (METI), Japan.

The JAEA recognises that microbial influences on the geological disposal of radioactive waste are still poorly understood. Consequently, it is undertaking ecological studies of samples from Horonobe and is obtaining information, which can be used in developing the MINT simulation model and the numerical geochemical code 'PHREEQ-C' (Parkhurst, and Appelo, 1999). These models are being used to assess microbial influences, which can be used in performance assessments. JAEA recognised the need to provide data derived from experimentation which can be used in these computer codes, particularly in relation how different microbial groups (e.g. methanogens, denitrifiers) influence geochemical and physical parameters and how these change with time.

Previously, the BGS provided information from batch experiments using Horonobe rock material which could be used for modelling microbial processes (Bateman *et al.*, 2009). The aim of the current study was to evaluate how biofilms, generated by denitrifying soil bacteria *Pseudomonas denitrificans*, influenced the flow of synthetic Horonobe groundwater through fractured Horonobe mudstone. Two experiments, one biotic and the other an abiotic control, were carried out using a flow-through column operated at a constant rate of fluid flow and under pressurised conditions. Changes in biological and chemical parameters were monitored throughout the experiment along with changes in confining pressure and temperature. On completion of the experiments, the columns were carefully dismantled and observations were made on the fracture surfaces. Starting material was also characterised.

The results from the experiments can be summarised:

- **Biological material was observed in the starting material and in material from the completed biotic experiment** but not from material from the completed abiotic experiment. The starting material appeared to be contaminated with fungal hyphae which occurred prior to its arrival at BGS. The observed biological material arising from the biotic experiments are different in nature to those seen in the starting material and we attribute this to the activity of *P. denitrificans* during the biotic experiment.
- Both the biotic and abiotic control experiments were of very short duration with injection of bacteria in the biotic experiment only over a period of 28 days. The results show that *P. denitrificans* can survive in the core material over this period and that total numbers appear to increase in the outflow fluid indicating that the environment within the core is conducive to the growth and activity of this organism. Clearly, ***P. denitrificans* can survive and thrive in the pressurised flow through column experiments** containing fractured material from Horonobe (flow rate of 300  $\mu\text{l hr}^{-1}$ ) when exposed to synthetic Horonobe groundwater (supplemented with sodium acetate at 0.2500 g l<sup>-1</sup> at JAEA's request) over a period of 28 days.

- Organic filaments covered the fracture surface from the biotic experiment together with *P. denitrificans* cells. **Thus a biofilm had formed in the columns injected with *P. denitrificans* although, given the short duration of the experiment, the biofilm was poorly formed.** These filaments appeared to be different to those observed in the starting material with clusters of microbial cellular structures present. In addition, some filaments appeared to consist of “strings” of elongate cells enclosed in an organic film or mucilage, whereas this was not seen in the starting material.
- **The features observed in the biotic experiment suggest that the bacteria produced filamentous biofilms** These filaments have utilised small microscopic channels in the fracture plane where tiny sub-parallel “ridges” and “troughs” formed as a result of shear along the fracture (i.e. slickensides) which create surface irregularities (or asperities) that do not fully interlock because of tiny displacement along the fracture surface. These represent potential fluid flow paths along the fracture. Similar microscopic channel-like fluid transport pathways were also exploited by the growth of fungi in the contaminated starting material.
- There was no petrographical evidence for the oxidation of pyrite or siderite in either the biotic experiment or the abiotic control experiment. However, **in the biotic experiment, the bacterial filaments had etched into the underlying rock substrate. The etching appeared to be non-specific with regard to surface mineralogy, affecting the silica-rich matrix, pyrite and siderite.** No alteration or dissolution effects were observed in the starting material or in the abiotic control experiment.
- Essentially, **there were very few changes in the fluid chemistry for both the biotic and abiotic experiments.** No significant differences were observed the chemistry of the outflow fluid from the biotic column when compared to the abiotic column. This implies that the duration of each test may not have been long enough to allow chemical changes to be observed.
- **Fluctuations in pressure profiles of the cores were detected by the transducers during the experiments.** Overall, the changes in pressure could be explained by partial clogging of conductive pathways which were then flushed as the hydraulic pressure locally increased. The resultant rapid saw-tooth like pressure profile observed in the biotic core during the experiment was symptomatic of a dynamic system exhibiting localised intermittent changes in permeability. However, the changes in pressure observed in the abiotic column were more likely to be the result of slow changes in flow geometry within the core giving rise to an overall change in permeability. Since the distinctive ‘spikes’ observed in the pressure graph of the biotic core material were not seen in the abiotic experiment, they may only be explained by the observed biofilm formation.

These experiments have generated a number of further questions and uncertainties. They were of very short duration and, consequently, there was little time for biofilm development to occur and thus for their impacts to be qualitatively measured. Nevertheless the observations from the experiment have shown that biofilms from *P. denitrificans* do form over a 28 day period and that physical etching of minerals is occurring. Additionally, an effective methodology has now been developed to gain robust data in any future experiments.

Minimal chemical information has been generated from this short-term study which can be used in a computer model (Tochigi *et al.*, 2007). Longer duration experiments (i.e. over a period of a year or more) are needed to obtain such data which would also yield information on the impacts of biofilms on fracture transport properties which is of great significance in understanding fluid movement in and around a repository. Long-term experiments will also allow equilibration of the experimental systems prior to injection of the perturbing organisms.

# 1 Introduction

The BioTran project was initiated to examine the effects of microbes on sub-surface transport processes, especially in the context of geological disposal of radioactive waste. Early work focussed on hard rock environments using dioritic material from the Äspö Underground Research Laboratory (URL). In 2008-2009, the scope of Biotran broadened to encompass batch experiments on mudstones, host rocks relevant to radioactive waste management in Japan. The current (2009-2010) BioTran work programme furthers this work by using column experiments to investigate the effects of microbes on fractured mudstone. This work was undertaken on behalf of the Japanese Atomic Energy Authority (JAEA) and part-funded by the Ministry of Economy, Trade and Industry of Japan (METI), Japan.

The JAEA recognises that microbial influences on the geological disposal of radioactive waste are still poorly understood. Consequently, it is undertaking ecological and microbiological studies of materials from Horonobe and is developing new evaluation methods. Currently, JAEA is undertaking ecological studies of samples from Horonobe and is obtaining information, which can be used in developing the MINT simulation model and the numerical geochemical code 'PHREEQ-C' (Parkhurst and Appelo, 1999). These models are being used to assess microbial influences, which can be used in performance assessments. The focus of BGS involvement is:

- to provide information from experiments using Horonobe rock material that can then be used for modelling microbial processes;
- to undertake a literature review to assess the impact of biofilms on transport processes in host rocks relevant to the Japanese radioactive waste management programme.

This report details the results from the recent column experiments.

In the previous 2008/2009 work programme, information was provided from short term (four week) batch experiments using rock material from Horonobe together with synthetic Horonobe groundwater and two microbial groups (methanogens and denitrifiers), (Bateman *et al.*, 2009). The results showed fluctuations in microbial numbers (although none appeared to be viable at the end of the experiments); but no changes were observed in fluid chemistry, mineralogy or surface areas. Additionally, no biological structures were observed at the end of the experiments.

As a consequence, JAEA requested that longer term experiments using column systems were performed as part of the work programme for 2009/2010. The work was started in September 2009 and completed in December 2009.

## 2 Column Experiments

The aim of the experiment was to evaluate how biofilms, generated by denitrifying soil bacteria *Pseudomonas denitrificans* (National Collection of Industrial and Marine Bacteria (NCIMB). 9496), influenced the flow of synthetic Horonobe groundwater through fractured Horonobe mudstone. The experiment used a flow-through column operated with a constant fluid flow and under pressurised conditions. The experiments were performed using intact sections of whole rock core from Horonobe which was supplied by Dr Kaz Aoki (JAEA) in August 2009, a denitrifying bacterial culture (*Pseudomonas denitrificans*) as specified by Dr Yoshikawa (JAEA), and a synthetic groundwater composition based upon information supplied by JAEA (Yoshikawa, per comm., Appendix 1).

The apparatus was fully assembled in September 2009 and injected with artificial groundwater on 30<sup>th</sup> September 2009. Injection with *P. denitrificans* for the biotic experiment started on 12<sup>th</sup> October 2009 and the experiment decommissioned on 9<sup>th</sup> November 2009. The abiotic experiment (i.e. no injection of microorganisms) started on 19<sup>th</sup> November 2009 and was decommissioned on 21<sup>st</sup> December 2009.

## 2.1 PREPARATION OF FLUIDS

The synthetic groundwater was prepared from laboratory grade reagents as shown in Table 1.

**Table 1 Composition of synthetic groundwater**

Reagent	weight used (g l <sup>-1</sup> )
NH <sub>4</sub> Cl	0.6519
NaHCO <sub>3</sub>	3.1528
FeCl <sub>3</sub> .6H <sub>2</sub> O	0.0133
KBr	0.1132
MnCl <sub>2</sub> .4H <sub>2</sub> O	0.0002
H <sub>3</sub> BO <sub>3</sub>	0.7778
KCl	0.1750
MgCl <sub>2</sub> .6H <sub>2</sub> O	0.9199
CaCl <sub>2</sub> .2H <sub>2</sub> O	0.3851
NaCl	10.3322
NaH <sub>2</sub> PO <sub>4</sub>	0.0063
Na <sub>2</sub> SO <sub>4</sub>	0.0030

Si was added as a 1000 mg l<sup>-1</sup> Si standard final [Si] = 25 mg l<sup>-1</sup>

Sodium acetate (CH<sub>3</sub>.COONa.H<sub>2</sub>O) was added as 0.2500 g l<sup>-1</sup> (TOC = 22 mg l<sup>-1</sup>) following discussion with JAEA. The fluid was then filter sterilised using a 0.2 µm filter and refrigerated until assembly of the experiment.

## 2.2 PREPARATION OF INTACT CORE MATERIAL

Two cores were taken at depths of 40.80–41.00 m and 90.04–90.24 m respectively. The cores were covered in protective wax and shipped from Japan by courier. On receipt, physical parameters, e.g. overall dimensions, orientation at sampling, location of fractures and other imperfections were recorded for each core before reference samples were taken for the mineralogical characterisation. Quantitative X-ray diffraction (XRD) analysis, BET surface area analysis and SEM analysis were performed on the starting material in addition to its geotechnical properties (grain density, etc.). The cores were re-drilled to produce a fresh surface and reduce the possibility of contamination from the original drilling fluids; each core was then cut using a saw to a suitable length to fit into the column assembly. The material sampled at 40 m depth was used for the biotic experiment as it had a naturally occurring longitudinal fracture. The 90 m material was used for the abiotic test, visually it did not appear to be fractured but once subjected to a sharp impact its friability gave rise to multiple longitudinal fracture surfaces. The orientation of the cores at sampling was reproduced when the material was loaded into the test rig.

## 2.3 BACTERIAL CULTURE

JAEA requested the use of the bacteria *Pseudomonas denitrificans* (the ‘Denitrifier’) in the column experiments. Using groundwater information from Horonobe, Tochigi et al. (2007) have shown that denitrifying bacteria are likely to be the group of organisms with the greatest activity.

Consequently, the impact of this group of organisms on Horonobe rock transport properties is the focus of the current study.

A freeze-dried culture of *Pseudomonas denitrificans* (NCIMB 9496) was received from NCIMB, UK and resuscitated in a recommended growth media, nutrient agar CM3 (Oxoid) and incubated at 25°C. The active growing cultures were then transferred into artificial groundwater ready for inoculation.

To prepare the cultures for inoculation, the active cultures were transferred to sterile 35 ml centrifuge tubes and centrifuged at 4600 rpm for 10 minutes. The supernatant was removed from each tube using sterile disposable pipettes and replaced with sterile synthetic groundwater. This process was repeated a further four times to ensure traces of the growth media were removed. Decreasing volumes of synthetic groundwater were added at each stage to concentrate the bacteria. The resulting fluid was then added to approximately 500 ml of synthetic groundwater, this produced sufficient volume to fill the syringe pump. A 1 ml sample of each suspended culture was removed by sterile pipette and preserved in gluteraldehyde fixative solution (Jass and Lappin-Scott, 1992) prior to microscopic examination. The total number of bacteria inoculated was then determined by direct counting using epifluorescence microscopy (Hobbie *et al.*, 1977; Jass and Lappin-Scott, 1992).

## 2.4 ANALYTICAL TECHNIQUES

Standard methods of analysis of solid and liquid samples were employed in this study. Prior to the start of this study, the bulk rock and clay mineralogy of the intact core material (samples taken at 40m and 90m depth) were characterised.

### 2.4.1 Mineralogical analysis

#### 2.4.1.1 QUANTITATIVE X-RAY DIFFRACTION

Bulk mineralogical analysis was carried out on the original Horonobe cores (40 m and 90 m) and on the post-experimental residues (biotic and abiotic) by X-ray diffraction (XRD) analysis using bulk-powdered samples. Material for XRD analysis was prepared as randomly orientated sample mounts. The principal mineralogical components were identified by comparison to reference diffraction data, and then quantified (for components other than clay minerals) by computer modelling the XRD diffraction profiles using the Rietveld refinement technique (Snyder and Bish, 1989).

Clay mineralogy was characterised by XRD analysis of the <2 µm fraction, separated from the disaggregated bulk rock material, by dispersion in water and sedimentation under Stoke's Law. The clay mineralogy was determined using orientated clay mineral XRD mounts. A representative portion of each sample was initially ground in a pestle and mortar. In order to achieve a finer and uniform particle size for whole-rock XRD analysis, c.2 g of each sample was wet-micronised under acetone for 10 minutes, taking care to exclude all traces of water. The micronised samples were then dried at 40°C, disaggregated and back-loaded into standard stainless steel sample holders for analysis.

For clay mineral XRD analysis approximately 5 g of each sample was dispersed in deionised water using a reciprocal shaker combined with ultrasound treatment. The suspensions were then sieved on 63 µm and the <63 µm materials placed in a measuring cylinder and allowed to stand. In order to prevent flocculation of the clay crystals, 1 ml of 0.1M 'Calgon' (sodium hexametaphosphate) was added to the suspensions. After a time period determined from Stokes' Law, a nominal <2 µm fraction was removed and dried at 55°C. 100 mg of the <2 µm material was then re-suspended in a minimum of distilled water and pipetted onto a ceramic tile in a

vacuum apparatus to produce oriented mounts. The mounts were Ca-saturated using 0.1M  $\text{CaCl}_2 \cdot 6\text{H}_2\text{O}$  solution, washed twice to remove excess reagent and allowed to dry overnight.

XRD analysis was carried out using a PANalytical X'Pert Pro series diffractometer equipped with a cobalt-target tube, X'Celerator detector and operated at 45kV and 40mA. Whole-rock samples were scanned from  $4.5\text{--}85^\circ 2\theta$  at  $2.76^\circ 2\theta/\text{minute}$ . The  $<2\ \mu\text{m}$  oriented mounts were scanned from  $2\text{--}40^\circ 2\theta$  at  $1^\circ 2\theta\ \text{min}^{-1}$  after air-drying, after glycol-solvation and after heating to  $550^\circ\text{C}$  for 2 hours. Diffraction data were initially analysed using PANalytical X'Pert Highscore Plus version 2.2a software coupled to the latest version of the International Centre for Diffraction Data (ICDD) database.

Following identification of the mineral species present in the samples, mineral quantification was achieved using the Rietveld refinement technique (e.g. Snyder and Bish, 1989) using PANalytical Highscore Plus software. This method avoids the need to produce synthetic mixtures and involves the least squares fitting of measured to calculated XRD profiles using a crystal structure databank. Errors for the quoted mineral concentrations are typically  $\pm 2.5\%$  for concentrations  $>60\ \text{wt}\%$ ,  $\pm 5\%$  for concentrations between 60 and 30 wt%,  $\pm 10\%$  for concentrations between 30 and 10 wt%,  $\pm 20\%$  for concentrations between 10 and 3 wt% and  $\pm 40\%$  for concentrations  $<3\ \text{wt}\%$  (Hillier et al., 2001). Where a phase was detected but its concentration was indicated to be below 0.5%, it is assigned a value of  $<0.5\%$ , since the error associated with quantification at such low levels becomes too large.

#### 2.4.1.2 BET SURFACE AREA ANALYSIS

BET surface area analysis was performed on crushed original core samples (40 m and 90 m) and the post-experimental residues (biotic and abiotic) using a Micromeritics Gemini VI surface area analyser. Surface area analyses were carried out using the multipoint BET/ $\text{N}_2$  method based on the quantity of gas that adsorbs as a single layer of molecules on a solid surface. One form of the BET equation (Brunauer *et al.*, 1938) that describes the adsorption of a gas upon a solid surface is:

$$\frac{(P/P\phi)}{V[1 - P/P\phi]} = \frac{1}{(VmC)} + \frac{\left[ \frac{(C-1)}{(VmC)} \right]}{P/P\phi}$$

where  $V$  is the volume (at standard temperature and pressure, STP) of gas adsorbed at pressure  $P$ ,  $P\phi$  the saturation pressure which is the vapour pressure of liquefied gas at the adsorbing temperature,  $V_m$  the volume of gas (STP) required to form an adsorbed monomolecular layer, and  $C$  a constant related to the energy of adsorption.

The surface area  $S$  of the sample giving the monolayer adsorbed gas volume  $V_m$  (STP) is then calculated from:

$$S = \frac{VmAN}{M}$$

where  $A$  is Avogadro's number which expresses the number of gas molecules in a mole of gas at standard conditions,  $M$  the molar volume of the gas, and  $N$  the area of each adsorbed gas molecule.

Approximately 1 g of each sample (40 m and 90 m) was loaded into a glass sample tube and heated at  $50^\circ\text{C}$  overnight in a vacuum oven. Immediately preceding surface area analysis, a sample was installed onto the sample port of the Gemini VI surface area analyzer. Nitrogen as adsorbate gas was then introduced into the tube immersed in liquid nitrogen at  $-196^\circ\text{C}$  to allow adsorption. The surface area was then calculated from adsorption values for five different

adsorption pressures for N<sub>2</sub>. The manufacturers claim analyses are typically better than 0.5% accuracy.

#### 2.4.1.3 OPTICAL AND SCANNING ELECTRON MICROSCOPY

The fracture surface mineralogy and morphological characteristics of the core samples were characterised by cryogenic and variable pressure (low vacuum) scanning electron microscopy (SEM) techniques. The identification of minerals was aided by the use of energy-dispersive X-ray microanalysis (EDXA) that was carried out simultaneously during SEM observation.

##### *Analysis of the fracture surface in the starting material*

A subsample of starting core material used in the flow-through column experiment was carefully prised open to expose a fresh fracture surface. A piece of this material, approximately 20 x 20 mm and containing the exposed fracture surface, was mounted onto a 50 mm diameter aluminium SEM stub using Leit-C conductive-carbon-cement. This was examined directly, and without coating the surface with carbon or gold, by variable pressure scanning electron microscopy (VPSEM)

VPSEM analysis was carried out using a LEO 435VP variable pressure digital scanning electron microscope instrument. The SEM instrument was equipped with an Everhart-Thornley type detector for secondary electron imaging (SEI) and a four-quadrant (4 diode-type) solid-state backscattered electron (BSE) imaging detector. The instrument was operated using a low vacuum of 0.4 torr, electron beam accelerating potential varying between 10 and 20 kV, and beam currents between 100 and 500 pA. Morphological images of the fracture surface were recorded under VPSEM conditions using backscattered scanning electron microscopy (BSEM) imaging. The BSEM images also discriminate the different mineral/phases exposed on the fracture surface, since image brightness (electron backscattering) is also proportional to the density and average atomic number of the phase being imaged (Goldstein *et al.*, 1981).

Phase/mineral identification was aided by qualitative observation of energy-dispersive X-ray spectra recorded simultaneously during SEM observation, using an Oxford Instruments INCA Energy 450 energy-dispersive X-ray microanalysis (EDXA) system fitted to the SEM instrument.

##### *Analysis of the post-experiment fracture surface*

###### *Initial sample photography*

The reacted core sample was photographed immediately after recovery from the experimental test rig. The core readily parted along the steeply inclined fracture, and both the whole core and the fracture surfaces were photographed. Low-magnification photographs were recorded at 10 megapixel resolution using a Pentax K200 digital camera mounted on a rigid stand and using the macrophotography facility. The core samples were also photographed at higher magnification using a Olympus SZX10 binocular stereomicroscope fitted with an Olympus XC30 dedicated high-resolution digital camera.

After photographing the reacted core, the fracture surfaces were then examined in detail by VPSEM and cryogenic scanning electron microscopy (cryoSEM) techniques. CryoSEM was carried out within 2 hours of opening the core sample. However, in order to prevent the sample drying out prior to cryoSEM and VPSEM analysis the material was stored, suspended above water, in a sealed vessel maintained at 5°C in a refrigerator.

##### *Variable pressure cryogenic scanning electron microscopy and backscattered electron imaging*

Initially sub-samples of the reacted fracture surface were examined by cryoSEM, as uncoated frozen SEM specimens, using the LEO435VP SEM instrument operated in variable pressure mode. The LEO435VP instrument was also equipped with an Oxford Instruments CT1500 cryogenic sample preparation and SEM transfer unit. This was coupled directly to the SEM chamber via an airlock, giving access to a cryogenically-cooled sample cold-stage within the SEM chamber. The cryogenic sample preparation system was cooled directly by liquid nitrogen and SEM cold-stage was cooled by liquid-nitrogen-cooled dry nitrogen gas.

Approximately 5 x 5 x 5 mm fragments of moist sample containing part of the fracture surface were carefully taken from the larger core sample using a fine chisel and lightweight hammer to gently break pieces off. The small sub-sampled fragments were mounted on gold-plated sample carrier that fits directly onto the cryogenic preparation chamber and SEM cold stages. The fragments were held in place by a small steel jaw clip mounted permanently on the sample carrier. The sample was then rapidly frozen by immersion in a melting mixture of solid and liquid nitrogen “slush” within liquid nitrogen in the CT1500 nitrogen slush-freezing unit. The frozen sample, on its sample carrier, was withdrawn under vacuum into a special vacuum-transfer vessel, and transferred under vacuum onto the cold-stage within the cryogenic sample preparation and SEM transfer unit, mounted on the side of the SEM chamber. This was maintained at a temperature of about -170°C. The frozen sample was then transferred via this system onto the cold stage inside the SEM chamber which was also maintained at a temperature of about -170°C.

The fracture surfaces were observed uncoated, using the SEM instrument under variable pressure (low vacuum) conditions with a chamber pressure of 0.3 to 0.4 torr, electron beam accelerating potential varying between 10 and 20 kV, and beam currents between 100-500 pA. Morphological images of the fracture surface were recorded under VPSEM conditions using BSEM imaging with BSEM. The surface of the sample was “developed” by warming the sample to about -80°C and slowly ablating the frozen porewater from the surface of the sample, to reveal the underlying frozen rock surface. When satisfied with the level of detailed revealed by ablating the ice, the sample was rapidly re-cooled to -170°C to stop further ablation.

#### *High vacuum cryogenic scanning electron microscopy and secondary electron imaging*

Higher-resolution cryoSEM observation of the fracture surfaces from the reacted core was also undertaken using a FEI Company QUANTA 600 environmental scanning electron microscope (ESEM) instrument equipped with a Gatan ALTO 2100 cryogenic sample preparation and SEM transfer unit. This was also fitted directly to the ESEM chamber, via an airlock, giving access to a cryogenically-cooled sample cold-stage within the ESEM chamber. As with the LEO 435VP – Oxford CT1500 instrument (see above) the ALTO 2100 cryogenic sample preparation system was cooled directly by liquid nitrogen with the cold-stage in the SEM chamber being cooled by liquid-nitrogen-cooled dry nitrogen gas. This instrument was also equipped with an Oxford Instruments fully-integrated INCA Energy 450 X-Max EDXA system (with large area 50 mm<sup>2</sup> Peltier-cooled silicon-drift detector (SSD)) and INCA Wave 700 wavelength-dispersive X-ray microanalysis system.

Small (5 x 5 x 5 mm) fragments of freshly broken material containing undisturbed fracture surface were taken as described above, and were mounted on a gold-plated brass carrier and held in place with a specially-designed jaw-vice built into the slide carrier. A small drop of cryogenic mounting compound (Tissue-Tek® O.C.T™ Compound - carbowax in polyvinyl alcohol solution) was used to fix the sample in place more firmly and to ensure good thermal contact on the cryogenic slide carrier. The sample was then rapidly frozen by immersion in a melting mixture of solid and liquid nitrogen “slush” within liquid nitrogen in the ALTO 2100 nitrogen slush-freezing unit. The frozen sample, on its sample carrier, was withdrawn under vacuum into a special vacuum-transfer vessel, and transferred under vacuum onto the cold-stage within the cryogenic sample preparation and SEM transfer unit, mounted on the side of the

ESEM chamber. This was maintained at a temperature of about  $-170^{\circ}\text{C}$ . The frozen sample was then transferred via this system onto the cold stage inside the ESEM chamber which was also maintained at a temperature of about  $-170^{\circ}\text{C}$ .

The fracture surfaces were initially observed uncoated, using the SEM instrument under high vacuum conditions with a chamber pressure of between  $2 \times 10^{-4}$  torr and  $1 \times 10^{-6}$  torr, electron beam accelerating potential varying between 5 and 10 kV, and low beam currents of between 0.8-2.0 pA. Morphological images of the fracture surface were recorded under High Vacuum SEM conditions using BSEM imaging. As with the cryoSEM analysis on the VPSEM system, the surface of the sample was “developed” by warming the sample to about  $-80^{\circ}\text{C}$  and slowly ablating the frozen porewater from the surface of the sample, to remove any films of water, and hoar frost condensed on the surface during the freezing process, reveal the underlying frozen rock surface. When satisfied with the level of detail revealed by ablating the ice, the sample was rapidly re-cooled to  $-170^{\circ}\text{C}$  to stop further ablation. After initial observations of the uncoated sample the frozen sample was transferred back onto the cold-stage of ALTO 2100 cryoSEM preparation chamber and coated with gold using an in-built sputter-coating device. The gold-coated frozen sample was then re-examined in the ESEM using SEI to obtain higher resolution SEM images.

#### *Environmental scanning electron microscopy with secondary and backscattered electron imaging*

High-resolution SEM observations were also made of the fracture surfaces from the reacted cores in the moist state, examined directly from the experiments were also carried out using ESEM, without cryogenic preparation. ESEM analysis was undertaken using the FEI Company QUANTA 600 ESEM instrument described earlier.

Relatively large (up to  $20 \times 10 \times 5$  mm) fragments of freshly broken material exposing the undisturbed fracture surface were mounted directly onto the aluminium sample stage in the ESEM instrument using a small piece of plasticine to hold the sample in place and in an appropriate orientation. The ESEM instrument was operated under a water vapour atmosphere at a pressure of 0.4 to 0.5 torr, under high vacuum conditions with a chamber pressure of between  $2 \times 10^{-4}$  torr and  $1 \times 10^{-6}$  torr, electron beam accelerating potential varying between 10 and 20 kV, and low beam currents of about 500 pA. Secondary electron images (SEI) were recorded using the specialised FEI Company low vacuum secondary electron LVSEM) detector rather than the conventional Evert-Thornley secondary electron detector. BSEM images were made using a solid-state diode-type detector.

## **2.4.2 Analysis of fluids**

### 2.4.2.1 MICROBIAL CHARACTERISATION

Microbial biomass was evaluated using epifluorescence microscopy. Epifluorescence microscopy uses a short wavelength transmission source to fluoresce a sample stained with the nucleic acid selective cationic fluorochrome. The fluorescent stain, Acridine Orange, or N,N,N',N'-tetramethylacridine 3,6-diamine ( $\text{C}_{17}\text{H}_{19}\text{N}_3$ ), was used to determine total cell counts (Hobbie *et al.*, 1977; Jass and Lappin-Scott, 1992). Acridine Orange is capable of permeating cells and interacting with DNA and RNA by intercalation or electrostatic attractions. When the fluorescent stain interacts with DNA, which is spectrally similar to fluorescein, the excitation maximum is at 502 nm (cyan) and the emission maximum at 525 nm (green), while RNA interactions shift the excitation maximum to 460 nm (blue) and the emission maximum to 650 nm (red). Thus, it is possible to determine if cells are metabolically active as they appear red due to the predominant RNA whereas inactive or slow growing bacterial have mostly DNA and

appear green. By examination of 20 randomly selected fields of view, the numbers of bacteria per ml can be counted.

#### 2.4.2.2 CHEMICAL ANALYSIS

A reference sample of the artificial groundwater used to fill the syringe pump was taken for comparison to the outflow fluids from the biotic and abiotic columns at the start of each test (day 0) and at 7 day intervals until the end of the experiments. Chemical analyses included major anions by ion chromatography, (IC) and cations by Inductively Coupled Plasma - Optical Emission Spectroscopy, (ICP-OES), as well as redox sensitive species ( $\text{Fe}^{2+}/\text{Fe}^{3+}$ ), pH and selected microbial nutrients (e.g. C, P, S and N). Non-Purgeable Organic Carbon (NPOC) was also evaluated which gives an indication of the degradation rate of organic compounds during the experiments.

### 2.5 EXPERIMENTAL DESIGN

The flow-through column experiments were performed using intact Horonobe rock core, containing naturally occurring longitudinal fractures. Core material was positioned vertically in a Teflon sheath with end caps allowing fluid flow through the column and the assembly was then placed in a pressure vessel. Schematics of the completed experimental rig with the pressure vessel and rock core assembly are shown in Figures 1 and 2. Once assembled, the pressure vessel was partially filled with deionised water and pressurised to 1250-1260 kPa. The synthetic Horonobe groundwater was used to fill the syringe pump and the flow rate was set at  $300 \mu\text{l hr}^{-1}$  ( $\sim 7.2 \text{ ml day}^{-1}$ ). The cores were not pre-saturated with artificial groundwater prior to the start of the experiment. The first ‘biotic’ column was injected with *P. denitrificans* after 11 days and the test was terminated after 39 days in total. The second ‘abiotic’ column was not injected with the organisms and the test was terminated after 31 days. Pressure transducers, shown in Figure 1 as PT 1 and PT 2, were used to monitor the pressure changes within the cores while the syringe pumps controlled the flow-rate. The transducer outputs were recorded, along with actual pressure measurements on a calibrated DRUCK DPI 610 pressure calibrator and this data were subsequently used to calibrate the pumps and transducers. Other variables (e.g. vessel temperature, air temperature and confining pressure) were also logged continuously during the course of the experiment. Fluid samples were collected by syringe at regular intervals for chemical and biological analyses.

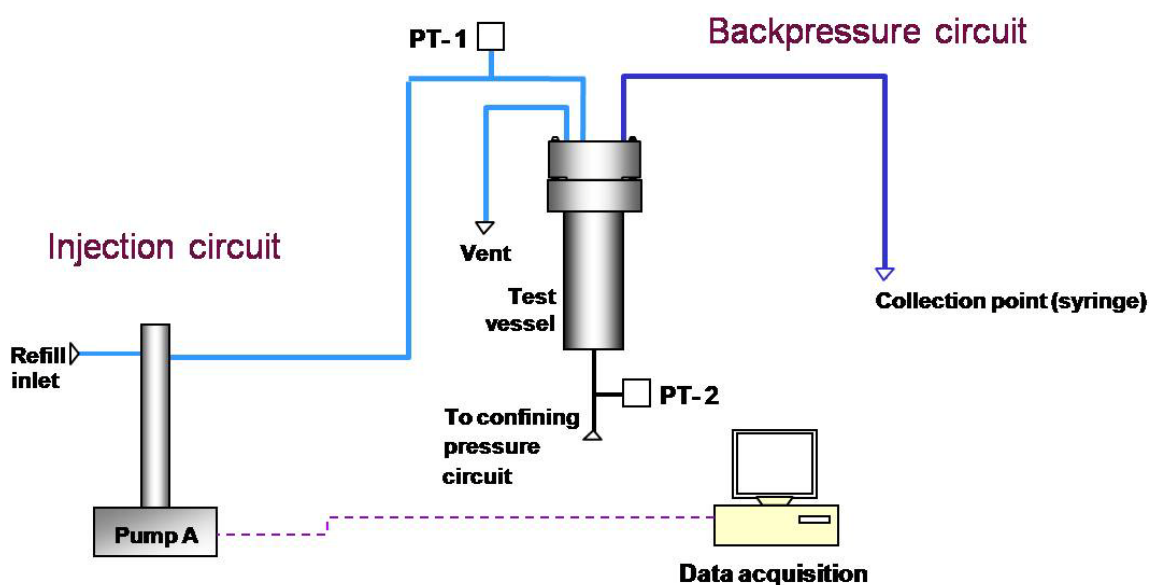


Figure 1 Schematic of column design.

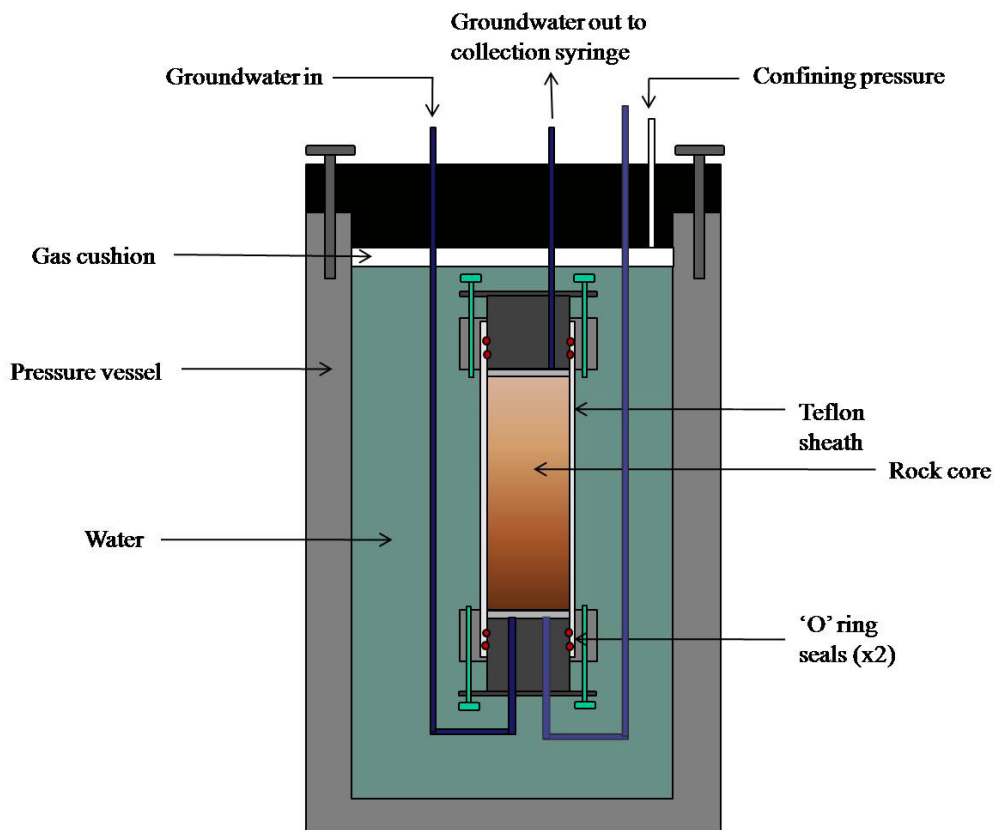


Figure 2 Schematic of pressure vessel with column containing rock core.

2.6 ASSEMBLY OF COLUMN EXPERIMENTS

For the biotic experiment, a section of the core (40 m depth) was prepared for analysis (Figure 3). The dimensions of the selected section, including the details of the fracture were recorded.

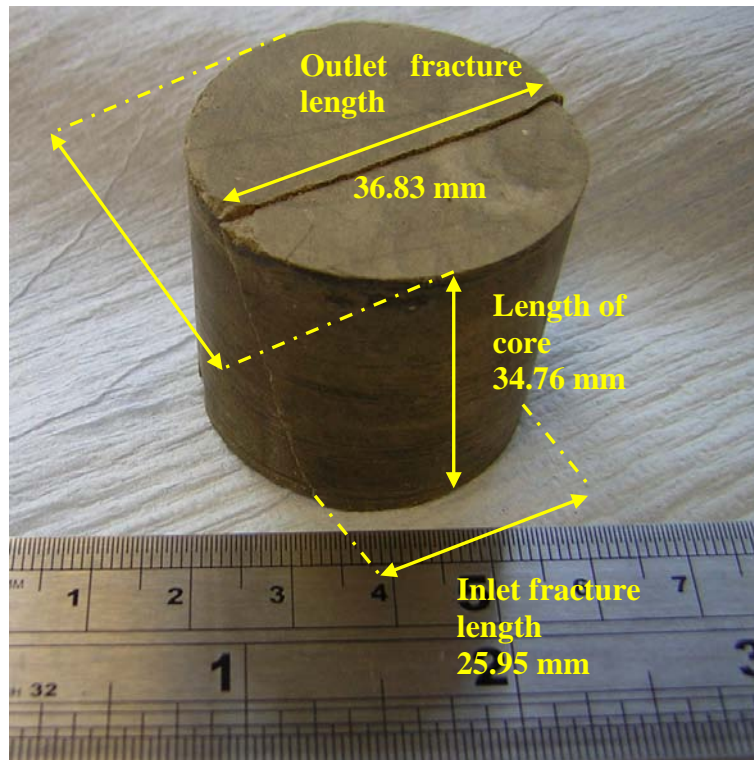
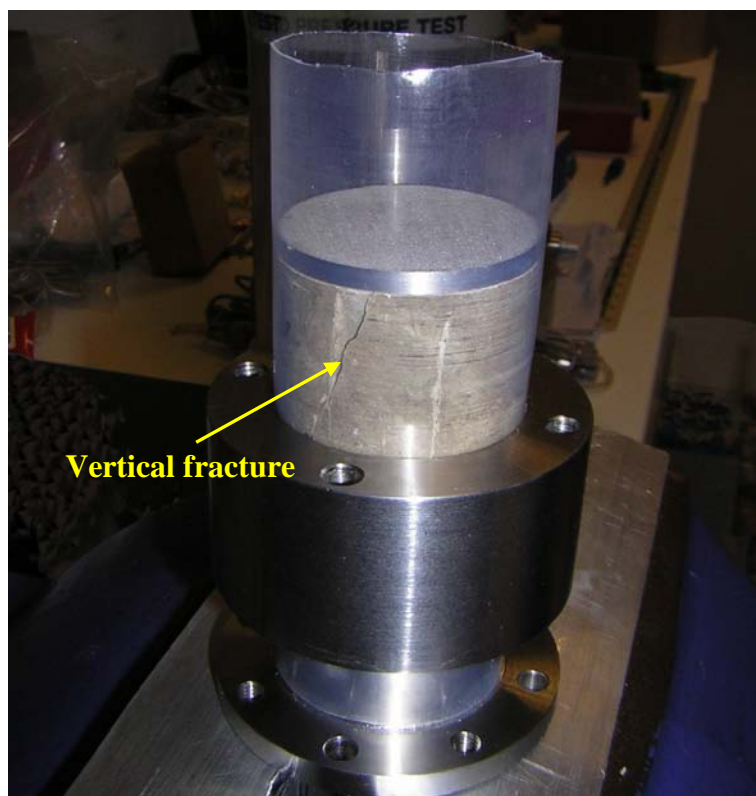


Figure 3 Core prior to emplacement in column. (Biotic experiment).

The fractured rock core was positioned vertically between the platens and enclosed in heat-shrink tubing. A hot air gun was used to shrink the tubing onto the rock and lower platen (Figures 4 and 5). The upper platen was removed and the locking ring positioned over the lower platen and 'O' rings to form a seal.



**Figure 4 Use of heat gun to shrink tubing around cut core. (Biotic experiment)**



**Figure 5 Close up of tubing around core showing fracture (Biotic experiment)**

The second locking ring was lowered over the core, the upper platen was replaced and the sleeve was heated to shrink the sleeve onto the upper platen. The second locking was positioned over the upper platen to form a seal with the upper 'O' rings. The completed assembly is shown in Figure 6.

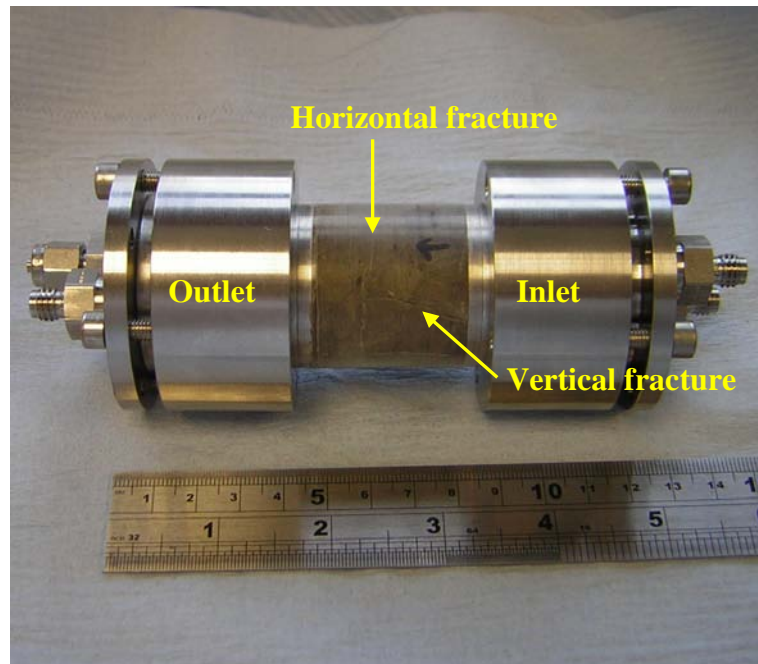


**Figure 6 Completed column prior to emplacement in pressure vessel. Note formation of lateral fracture which occurred during preparation (Biotic experiment).**

During assembly of the unit, in addition to the longitudinal fracture, a lateral fracture occurred along a bedding plane of the core (Figure 6), this fracture occurred 21.456 mm from the inlet. The unit is shown connected to the lid of the pressure vessel before inverting the assembly and placing inside the pressure vessel (Figure 7).

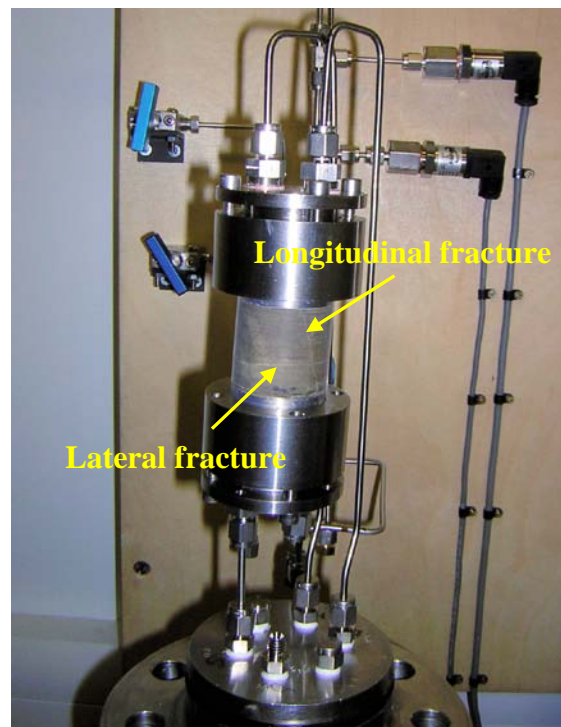


**Figure 7 Assembly prior to inversion and placement into pressure vessel (Biotic experiment).**



**Figure 8 Fully completed apparatus showing the attached pump assembly (Biotic experiment).**

The system is shown fully assembled in the test rig in Figure 8. The pressure vessel was partially filled with deionised water and pressurised. Artificial groundwater was used to fill the syringe pump and the flow rate was set at  $300 \mu\text{l hr}^{-1}$  ( $\sim 7.2 \text{ ml day}^{-1}$ ). The same methodology was used for constructing the abiotic experiment. The external dimension of the abiotic core closely resembled that of the biotic core. Accurate measurements of the abiotic core could not be made due to the friability and extensive fracturing of the material. The flow rate for the abiotic experiment was identical to the biotic core,  $300 \mu\text{l hr}^{-1}$  ( $\sim 7.2 \text{ ml day}^{-1}$ ).

## 2.7 DECOMMISSIONING OF COLUMN EXPERIMENTS

Figures 9 – 12 show the column apparatus after removal from the pressure vessel (Biotic experiment).



**Figure 9 Assembly after removal from pressure vessel (Biotic experiment)**

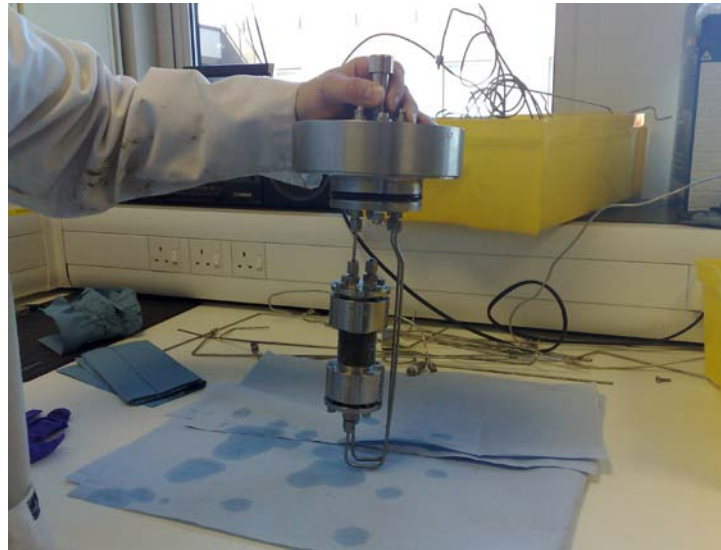


**Figure 10 Further view of assembly after removal from pressure vessel (Biotic experiment)**



**Figure 11 Column after removal from platen. Arrow shows direction of fluid flow during the experiment (Biotic experiment)**

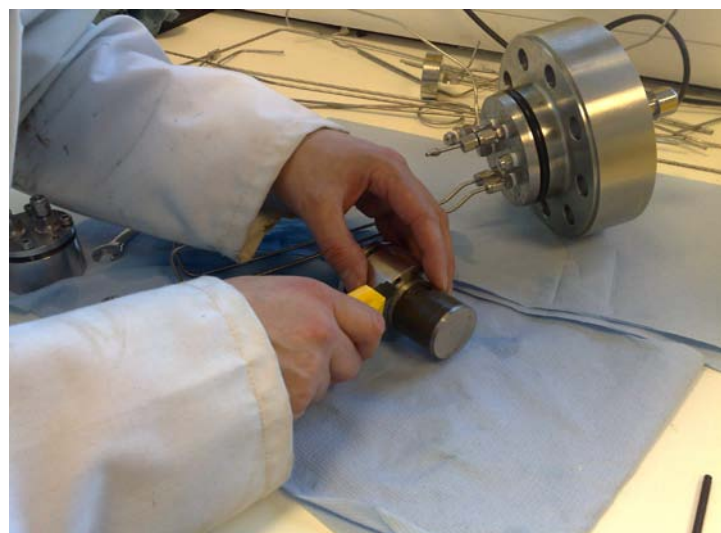


**Figure 12 Removal of second platen (Biotic experiment)**

### 3 Results – Physical Measurements

Both biotic and abiotic experiments were performed at a constant flow rate and changes in injection and confining pressure were continuously logged by pressure transducers during the tests. The resulting data are depicted graphically in Figure 13 (biotic experiment) and Figure 14 (abiotic control experiment). Any factors which could have affected the experiment, e.g. changes in external conditions were noted and an evaluation was made to determine if these timed events could be correlated to changes within the laboratory or the cores.

#### 3.1 BIOTIC CORE

Sterile artificial groundwater was pumped through the core assembly for a nominal period (11 days) commencing on 30<sup>th</sup> September 2009. The pump was stopped on 12 October 2009, which caused a brief dip in pressure (depicted graphically in Figure 13) and the sterile water was replaced with 500 ml of water inoculated with the *P. denitrificans* bacteria. The bacteria were injected when the pump was restarted and the experiment was terminated after 39 days on 9<sup>th</sup> November 2009.

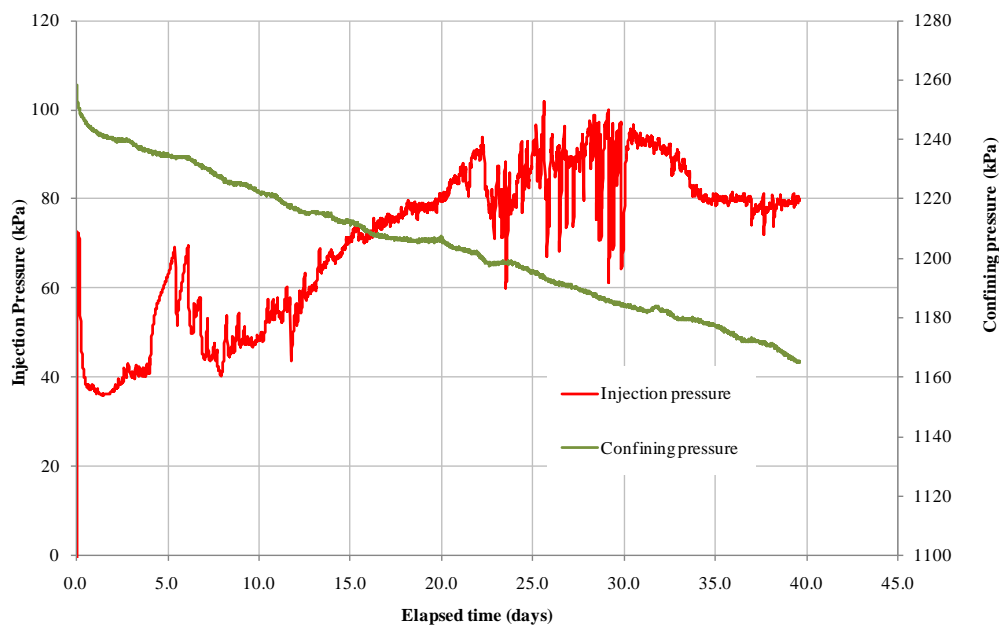


**Figure 13 Biotic experiment: injection and confining pressure data plotted against experiment duration in days**

At the start of the experiment a sharp increase in injection pressure was observed starting at 41 kPa (3.9 days) and rising to 69 kPa (5.3 days). At 5.5 days, the pressure decreases rapidly to 50 kPa. This pattern in the pressure profile occurred a second time when a maximum of 69 kPa was reached at 6 days before decreasing to 51 kPa at 6.3 days. As the bacteria were not injected until 11 days, changes in the permeability of the core may have been caused by the movement of fines. Blocking of the pore spaces by fine grained material would cause a localised increase in pressure and since the flow was maintained at a constant rate, breakthrough would occur as the pressure rose and new pathways were established. The pressure profile showed a gradual but steady increase from day 8 to day 23, although a dip was observed when the bacteria are injected at day 11. From day 23 to 30, the pressure averages around 88 kPa. However, the intermittent pressure ‘spikes’ observed at this time may have been the result of either transducer noise or

from further substantial changes in flow geometry. Due to the fracture, the material was highly permeable (i.e. the pressure within the core was low) and the pressure changes observed fell within the specified noise tolerance of the transducers. Transducer noise is caused by a poor electrical connection and is generally recorded as rapidly occurring spikes in the pressure data log. However, in this experiment, quiescent periods in the data were bracketed by pressure maxima and minima spanning time periods of several hours. In addition, this pressure pattern was only observed in the biotic core. It was therefore more likely to be the result of microbial activity causing partial blocking of the pore spaces with biological material. From day 30 to day 35, a gradual decrease in pressure was observed. From 35 days onwards the transducer response showed signs of a stabilisation in pressure of 80 kPa, thereafter the system began to oscillate in a quasi-steady state. The term quasi-steady describes a system where some parameters are fluctuating or not fully evolved but is close to achieving a steady state (a condition where all the variables remain constant and unchanging over time).

Overall, the short but rapid changes in pressure could be explained by partial clogging of conductive pathways either by fines, biofilm or a combination of both, which were then flushed as the hydraulic pressure locally increased. The resultant saw-tooth like pressure profile observed in the biotic core during the experiment was symptomatic of a dynamic system exhibiting localised intermittent changes in permeability.

### 3.2 ABIOTIC CORE

The abiotic column experiment ran for 31 days in total commencing on 19<sup>th</sup> November 2009 with no injection of organisms. The experiment was decommissioned on 21<sup>st</sup> December 2009. As with the biotic experiment, pressure changes were continuously monitored throughout the course of the test.

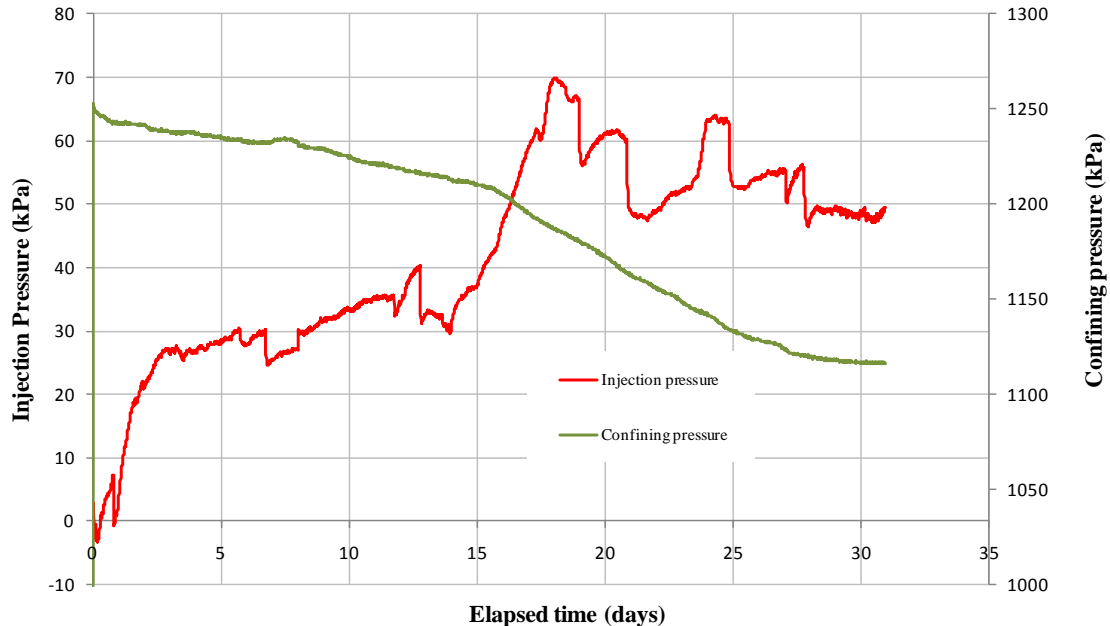


**Figure 14 Abiotic experiment: injection and confining pressure data plotted against experiment duration in days**

Figure 14 shows that the maximum pressure achieved within the abiotic core was 70 kPa at 18 days; this was marginally lower than the biotic core which achieved a maximum of 102 kPa at 25.6 days. A gradual increase in pressure was observed in the abiotic core between 0 and 3 days, followed by an inflection in the pressure curve and a reduction in the rate of pressure change. From 3 days to 15 days the transducer response showed signs of a pressure stabilisation at

around  $32 \pm 5$  kPa. From 15 days onwards, the resistance to flow spontaneously increases which may be caused by either localised blockages along conductive pathways or mechanisms associated with self-sealing, commonly observed in mud rocks (e.g. Cuss *et al.*, 2006; Horseman *et al.*, 2005). From 28 days onwards the transducer response showed signs of a pressure stabilisation at around  $49 \pm 3$  kPa, thereafter the system again appears to begin to oscillate in a quasi-steady state.

The changes observed during the first three days of the abiotic column experiment may relate to the movement of water into pore spaces during the initial pressurisation of the system. The fact that this was not observed in the biotic core may have been due to differences in fracture geometry between the two test samples. The abiotic core was of higher permeability than the biotic core as it contained multiple fractures and this was shown by the considerably lower maximum pressure of 70 kPa achieved by the abiotic column system. The differences in pressure profiles between the two cores highlight the variability of such samples and the impact this may have on test results.

Several changes in pressure were observed during the course of the abiotic column experiment and despite most being within the noise of the pressure transducers, it was more likely to be the result of slow changes in flow geometry within the core giving rise to an overall change in permeability. From day 28 onwards, it was possible that the core was on the verge of achieving a quasi steady-state but this could not be confirmed as the experiment ended on day 31.

## 4 Results – Fluids

### 4.1 MICROBIOLOGY

After 11 days, the sterile synthetic fluid injected into the ‘biotic’ column experiment was inoculated with  $1.18 \times 10^5$  ( $8.88 \times 10^3$  SE) bacteria  $\text{ml}^{-1}$  of *P. denitrificans*. The fluid was then passed through the core for a further 28 days. Samples of outflow fluid were taken at intervals and the mean numbers for total bacterial counts were determined by epifluorescence microscopy and given in Table 2. Results are only given for the biotic experiment as no bacteria were detected in the abiotic experiment.

**Table 2 Mean total counts of bacteria by epifluorescence microscopy (Biotic experiment)**

Outflow fluid Bacteria $\text{ml}^{-1}$	Standard error (SE)	Comments
0	n/a	Outflow (start up fluid)
0	n/a	Outflow prior to inoculation
0	n/a	7 days after inoculation
8.64E+05	6.68E+04	14 days after inoculation
5.11E+05	4.33E+04	21 days after inoculation
4.48E+05	7.07E+04	28 days after inoculation

These show that no organisms were present in the outflow 7 days after injection but the numbers of organisms present in the outflow after 14 days was greater than those injected into the core. Thus the time for transit of the bacteria through the core is between 7 and 14 days. However, the numbers decline to  $4.48 \times 10^5$  bacteria  $\text{ml}^{-1}$  after 28 days, although this is still higher than the count at injection. To establish if the bacteria were still viable at the end of the experiment, the total bacterial counts of the fluid remaining in the syringe pump was also determined. The fluid

was found to contain  $6.48 \times 10^8$  bacteria  $\text{ml}^{-1}$  (SE,  $6.96 \times 10^7$  bacteria  $\text{ml}^{-1}$ ), of which 10% were considered to be viable.

## 4.2 FLUID CHEMISTRY

The results of the fluid chemistry analysis for the biotic and abiotic experiments are tabulated in Appendix 2. No significant differences were observed the chemistry of the outflow fluid from the biotic column when compared to the abiotic column. This implies that the duration of each test may not have been long enough to allow chemical changes to be observed. Nevertheless, the concentrations of organic carbon (NPOC) decreased in the biotic core experiment from  $62.5 \text{ mg l}^{-1}$  (day 0) to  $30.5 \text{ mg l}^{-1}$  (11 days), the concentration then stabilised at around  $30 \text{ mg l}^{-1}$  until the end of the experiment (day 33). However, it is interesting to note that in the abiotic experiment the concentration of NPOC is three orders of magnitude greater than in the biotic experiment and that this also reduces in concentration over the duration of the study from  $6370 \text{ mg l}^{-1}$  (day 0) to  $4215 \text{ mg l}^{-1}$  (day 30). This implies that the concentrations of NPOC vary greatly in the Horonobe core material.

# 5 Results – Solid materials

## 5.1 WHOLE ROCK MINERALOGICAL ANALYSIS

The results of whole-rock XRD analyses are summarised in Table 3 and labelled XRD traces are shown in the Appendix 3.

The initial rock samples (taken at 40m and 90m depth) have similar mineralogies with major amounts of quartz (mean *c.* 39.8 %), albite (mean *c.* 19.8 %) and ‘mica’ (undifferentiated mica species possibly including muscovite, biotite, illite, illite/smectite etc.; mean *c.* 22.0 %) and minor/trace amounts of K-feldspar, ‘kaolin’ (one of the kaolin group minerals including halloysite, kaolinite etc.), chlorite, pyrite and smectite.

**Table 3 Summary of quantitative whole-rock XRD analyses**

Mineral	Original core		Post-experimental	
	(40 m)	(90 m)	(40 m)	(90 m)
Albite	20.0	19.6	20.1	19.3
Chlorite	2.6	1.9	1.6	1.9
Halite	<0.5	<0.5	0.9	1.6
‘Kaolin’	2.1	2.9	2.3	2.5
K-feldspar	8.7	7.4	8.6	7.2
‘Mica’	22.1	21.8	21.3	21.8
Pyrite	2.4	2.9	2.1	2.3
Quartz	39.2	40.4	40.0	40.8
Smectite	2.9	3.1	3.1	2.6

### KEY

‘nd’ not detected

‘mica’ = undifferentiated mica species including muscovite, biotite, illite and illite/smectite etc.

‘kaolin’ = one of the kaolin group minerals including halloysite, kaolinite etc.

The sample traces obtained from XRD analyses also showed broad peaks between 20-35°2 $\theta$ . Poorly ordered materials such as glasses or opaline silica species typically produce such broad features.

Halite was not detected in the starting material but was observed as a minor to trace component in both the biotic and abiotic reaction residues. This is an artefact of the sample preparation, and is derived from sodium chloride precipitated from the residual saline pore fluid (used as the experimental fluid) during freeze-drying of the sample.

In general, no evidence of any mineralogical changes in the sample due to bacterial interactions was observed in the experimental residue. The differences in clay mineral quantities that were observed between original sample core and the post-experimental biotic material may be due to bacterial interaction. However, this variation is more likely to be explained by sample heterogeneity and/or by the given quantification method where mineral concentrations below 3 wt.-% (Hillier *et al.*, 2001) have given errors of typically  $\pm 40$  %.

## 5.2 CLAY MINERAL OBSERVATIONS

XRD analysis of the <2  $\mu\text{m}$  materials showed that the clay mineralogy of the starting materials was predominantly composed of illite and smectite and only small proportions of kaolinite and chlorite. Quartz and albite were also identified in the <2  $\mu\text{m}$  fractions of the samples.

### ‘Non-swelling clays’

The non-swelling clays include illite, kaolinite and chlorite. Illite was identified by its characteristic air-dry  $d_{001}$  spacing of  $c.10.0\text{\AA}$  which remains invariant after glycol-solvation and heating. Kaolinite was identified by its characteristic air-dry basal spacings of  $c.7.1$  and  $3.58\text{\AA}$  which remain invariant after glycol-solvation but which disappear after heating at  $550^\circ\text{C}$  due to the meta-kaolinite’s X-ray amorphous state. Chlorite was identified by its characteristic air-dry and glycol-solvated basal spacing peaks at 14.2, 7.1, 4.73 and  $3.54\text{\AA}$  and particularly the presence of a peak at  $c.13.9\text{\AA}$  after heating at  $550^\circ\text{C}$ .

### ‘Swelling clays’

The swelling clay smectite was identified by its typical air-dry  $d_{001}$  spacing of  $c.14.5\text{\AA}$  which expands to a similarly typical  $c.17\text{\AA}$  on glycol-solvation and collapses under heating to  $550^\circ\text{C}$  for 2 hours to an ‘illite-like’  $10\text{\AA}$   $d_{001}$  spacing.

## 5.3 BET SURFACE AREA ANALYSIS

The results of BET/nitrogen surface area analyses are shown in Table 4. The original core samples have similar surface areas,  $c. 21.88 \text{ m}^2/\text{g}$  at 40 m depth and  $c. 24.07 \text{ m}^2/\text{g}$  at 90 m depth respectively.

**Table 4 Summary of BET/nitrogen surface area analyses**

Sample description	Surface area ( $\text{m}^2 \text{ g}^{-1}$ )
Original core at 40 m	21.88
Original core at 90 m	24.07
Post experimental material (biotic)	22.08
Post experimental material (abiotic)	24.42

Analyses of the post-experimental cores from both biotic and abiotic experiments do not show any significant change in surface area.

## 5.4 OPTICAL AND SCANNING ELECTRON MICROSCOPY OBSERVATIONS

### 5.4.1 Starting material

Petrographical observation by VPSEM of the starting material showed that the surface of the steeply-inclined fracture running the length of the core sample was completely unmineralised. The rock was seen to be highly siliceous: composed largely of silt-sized fragments of diatoms with delicate microporous skeletal frameworks of silica, fine sand-grade siliceous cylindrical sponge spicule fragments (Plate 1). A proportion of the diatom detritus includes relatively complete cylindrical forms (Plate 2). Subordinate detrital components include angular silt-grade grains of quartz and irregular silt-grade aggregates of illitic clay (Plate 1). Minor detrital silt-grade angular grains K-feldspar and plagioclase (probably of albitic to oligoclasic composition), and minor to trace muscovite are also present (Plate 1).

Fine grained authigenic pyrite is a significant component of the rock matrix, and fresh pyrite is also exposed in the fracture surface. The pyrite occurs either as framboidal aggregates in “clusters” or “pods” up to 100  $\mu\text{m}$  diameter (Plate 3) or as fine octahedral crystals ( $< 5 \mu\text{m}$  diameter) disseminated through the clay-silt-grade matrix (Plate 2). Minor siderite (magnesiosiderite ( $[\text{Mg,Fe}]\text{CO}_3$ ) in composition) is also present as an authigenic phase. It occurs disseminated as small rhombs (up to 10  $\mu\text{m}$ ), and can be found forming a replacive matrix cement lining the walls of burrow-like trace fossils. These burrow trace fossils can be seen as diffuse pale grey to buff-coloured features in hand-specimen.

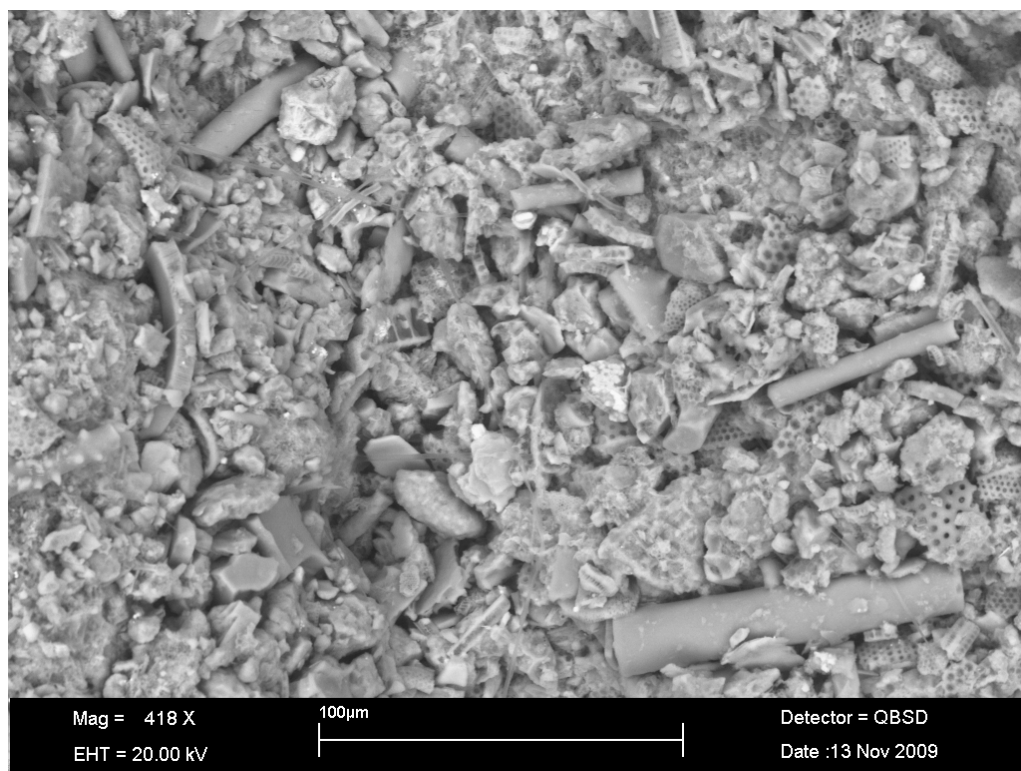


**Plate 1 BSEM image (from VPSEM) showing the morphology and mineralogy of the fracture surface in the starting material. Angular fragments of microporous siliceous diatoms make up a large part of the sample. Fragments of cylindrical siliceous sponge spicules, together with angular detrital quartz silt grains and irregular silt-grade aggregates of detrital illitic clay can also be seen. (Starting material). LEO 435VP SEM instrument.**

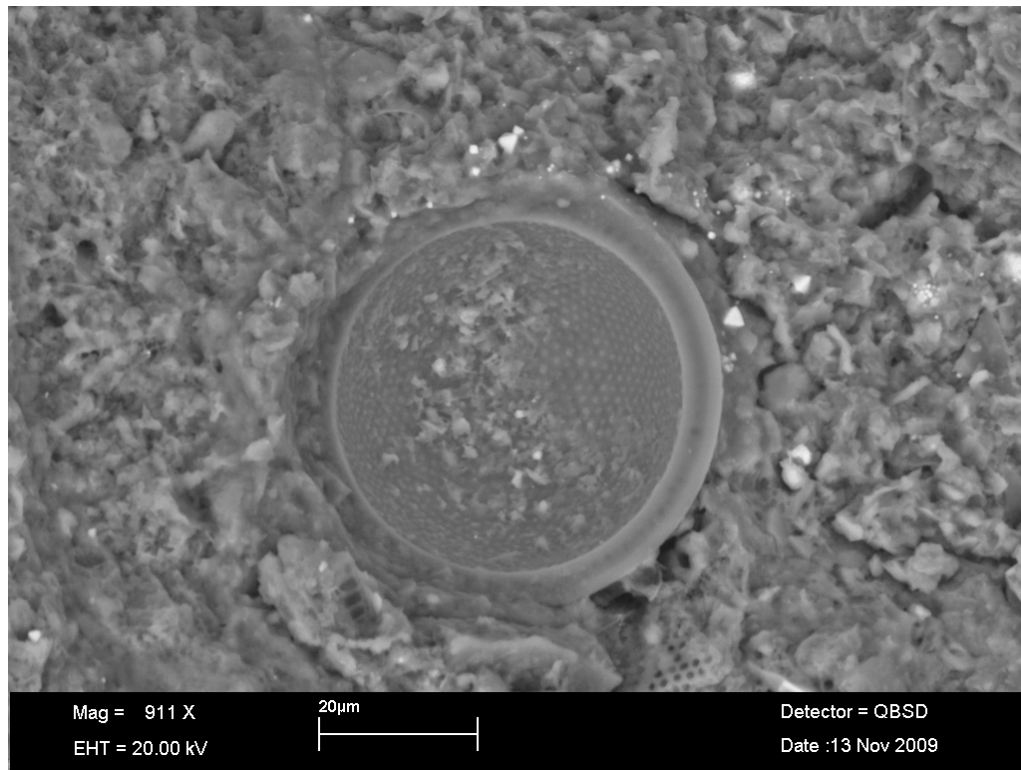


**Plate 2 BSEM image (from VPSEM) showing relatively large and complete cylindrical siliceous diatom skeleton with a compact groundmass of detrital clay, amorphous siliceous material and finer diatomaceous detritus. Fine bright grains of disseminated pyrite, with octahedral crystal forms, can be seen disseminated in the matrix. (Starting material).**

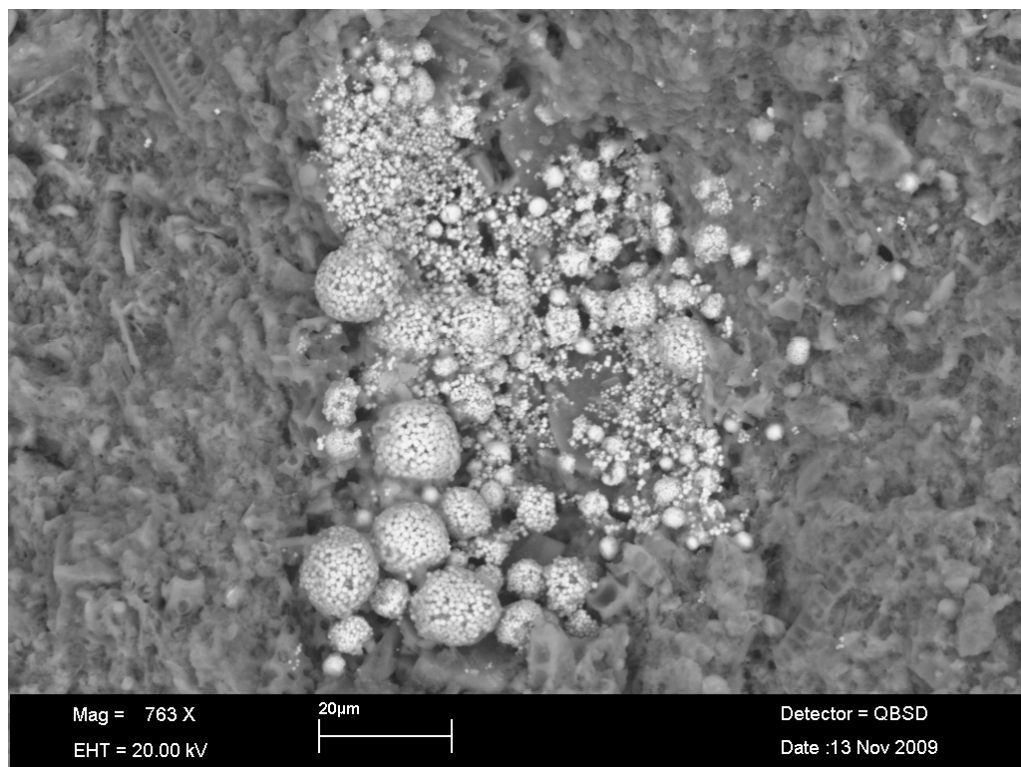


**Plate 3 BSEM image (from VPSEM) showing framboidal aggregates of fine grained pyrite forming a discrete "pod" within the siliceous diatomaceous matrix. (Starting material). LEO 435VP SEM instrument.**

Detailed examination of the fracture surface revealed a series of fine-scale “ridge and furrow” lination structures across the whole fracture surface (Plate 4 and Plate 5). These features are characterised by a steep “scarp” and a gentler “tail” slope, all aligned in the same direction, forming a series of small “steps” in the surface. The amplitude, from base of the furrow to top of the ridge” is of the order of 50 to 100  $\mu\text{m}$ . These features form an interconnected network of fine sub-parallel to anastomosing tubular channels along the plane of the fracture. The morphology of these features, with aligned “crag” and “tail” slope surfaces suggests that these are probably features formed by shear-deformation parallel to the fracture surface (i.e. slickensides)

VPSEM observations also showed that within these channels formed by the slickensides, loose silt particles were often present (Plate 6). Furthermore, fine organic filaments about 1-2  $\mu\text{m}$  diameter were found to be present across the whole fracture surface. These filaments form an interconnected mesh and penetrate along the slickenside channels in the fracture surface (Plate 7 and Plate 8). No cellular structure was observed in the filaments and they appear to have shrunk and collapsed, possibly as a result of drying during sample preparation and under vacuum in the SEM instrument during VPSEM observation. In morphology, these features closely resemble fungal hyphal structures although it is not possible to give a definite identification without further examination of intact core which is beyond the remit of the current study.

No evidence of mineralogical alteration of the fracture surface could be seen to be associated with these organic filaments. The surfaces of redox-sensitive minerals such as pyrite and siderite-magnesiosiderite were seen to be fresh and unaffected by oxidation products such as iron oxides or other alteration effects.

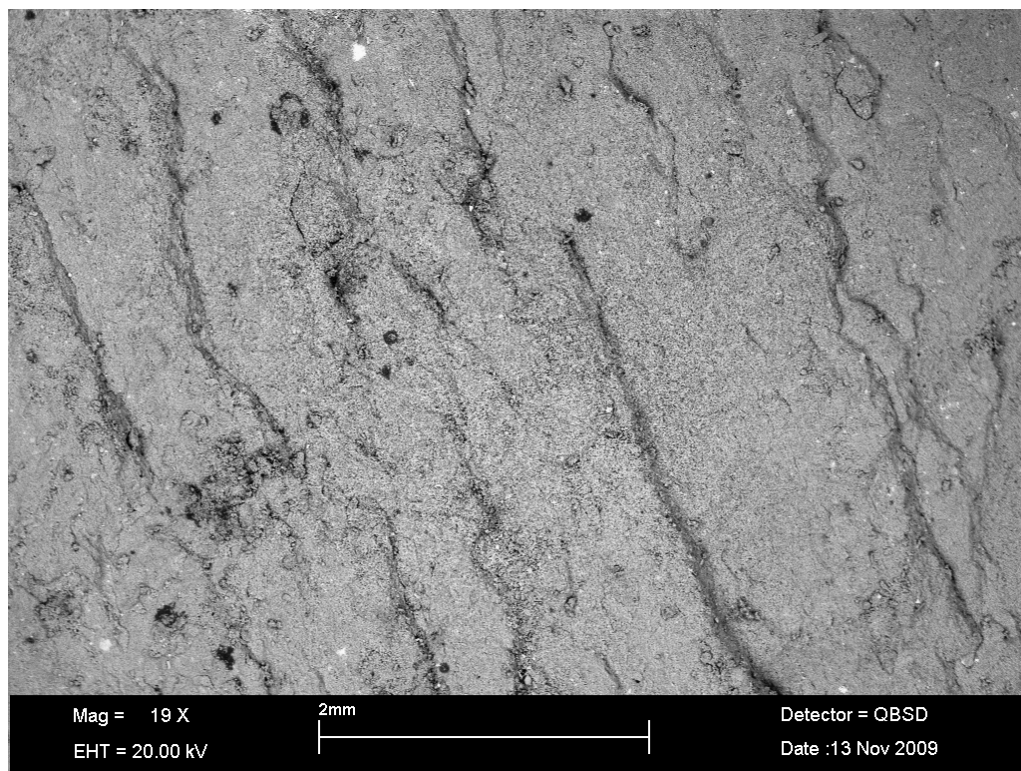


**Plate 4 BSEM image (from VPSEM) showing fine “ridge-and-furrow” ornamentation (with steeper “scarp” and gentler “tail” slopes) forming an interconnected network of sub-parallel to anastomosing fine channels along the fracture plane. (Starting material). LEO 435VP SEM instrument.**

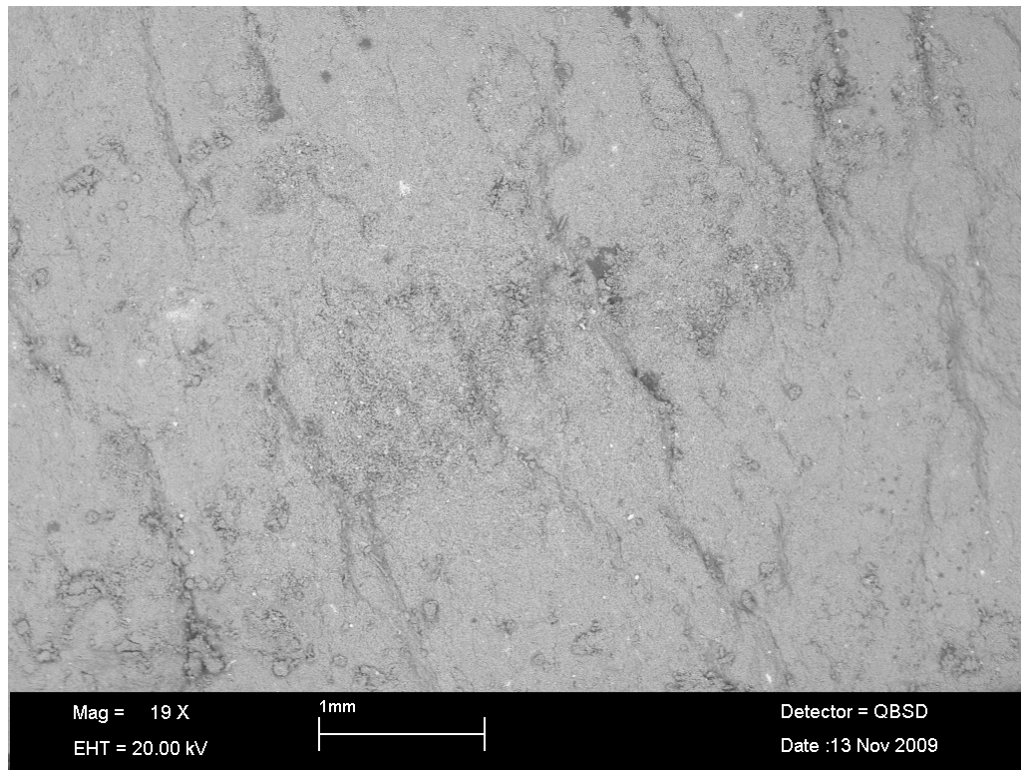


**Plate 5 BSEM image (from VPSEM) showing fine “ridge-and-furrow” ornamentation (with steeper “scarp” and gentler “tail” slopes) forming an interconnected network of sub-parallel to anastomosing fine channels along the fracture plane. (Starting material). LEO 435VP SEM instrument.**

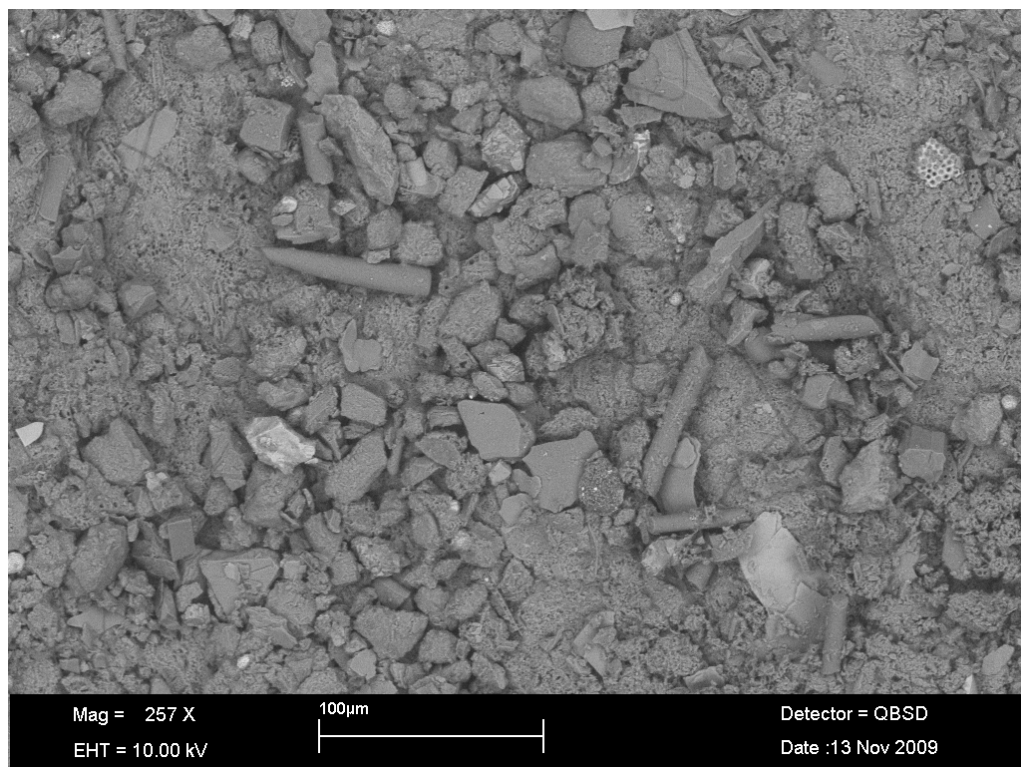


**Plate 6 BSEM image (from VPSEM) showing fine silt particles accumulated within the channels formed by the “ridge-and-furrow” lineaments on the fracture surface. (Starting material). LEO 435VP SEM instrument.**

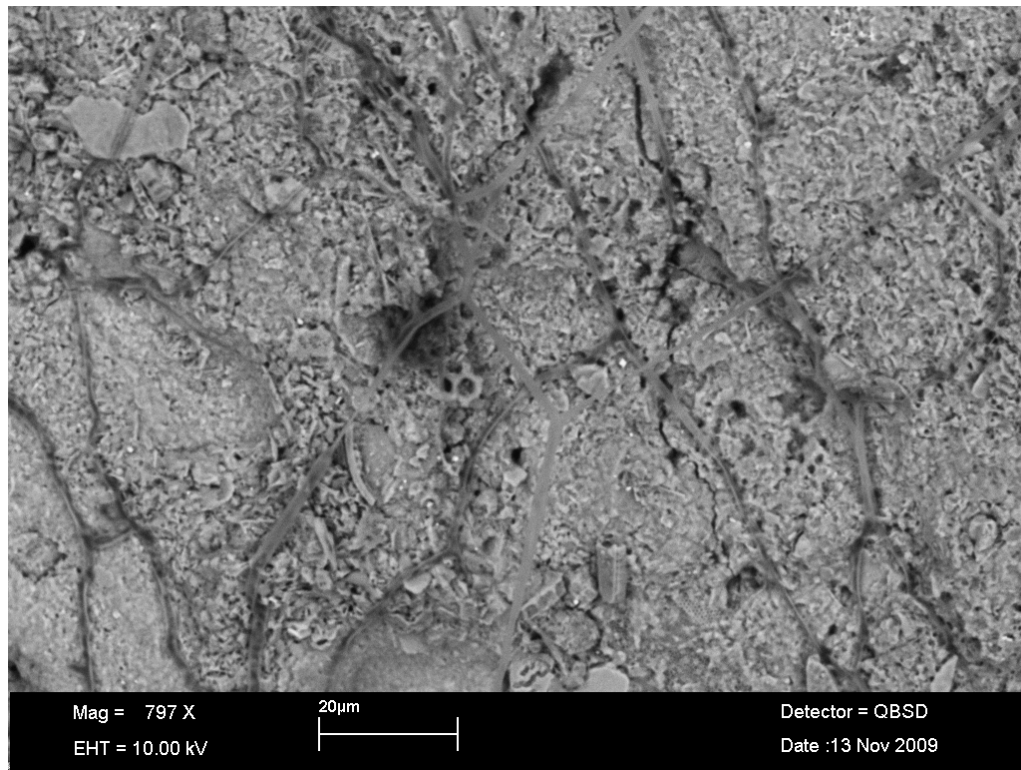


**Plate 7 BSEM image (from VPSEM) showing network of fine organic filaments (possibly fungal hyphae) growing across the fracture surface, following and penetrating along the interconnected network of sub-parallel to anastomosing fine slickenside channels in the fracture plane. (Starting material). LEO 435VP SEM instrument.**

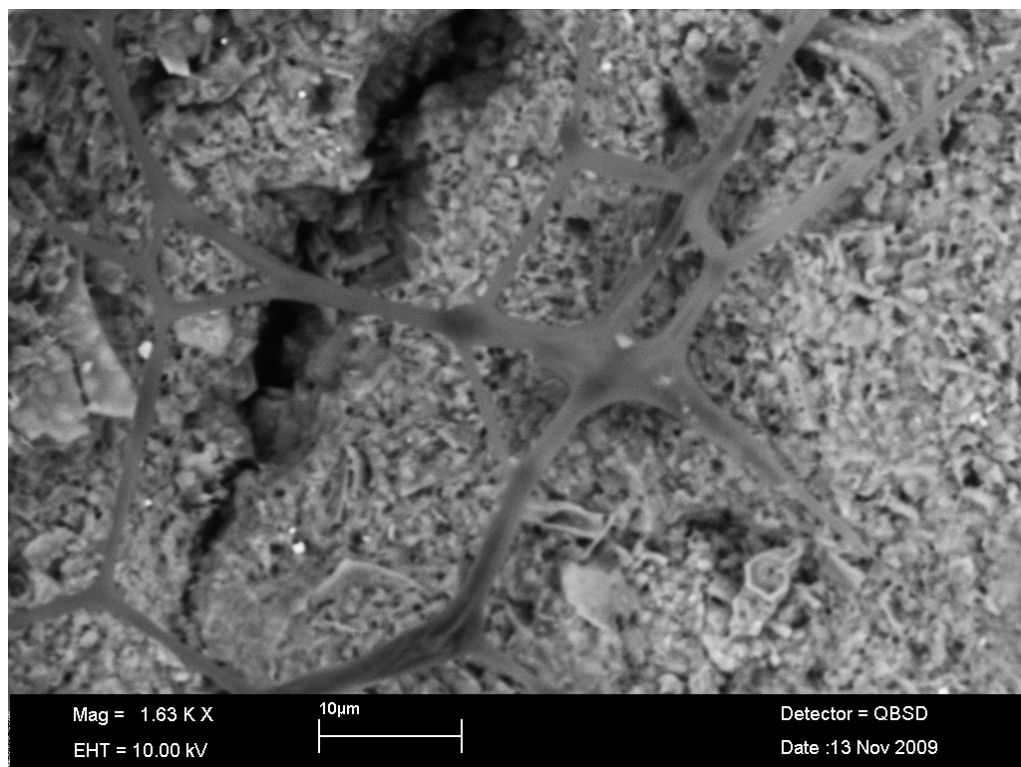


**Plate 8 BSEM image (from VPSEM) showing detail of the fine organic filaments coating the fracture plane. (Starting material). LEO 435VP SEM instrument.**

These observations clearly show that the core material provided by JAEA was already microbially-contaminated and that fungi appear to be already in the fracture at the start of the experiment. BGS experience has found that cores samples containing organic-rich materials (e.g. coals, oil-shales, organic-rich clays) are commonly found to contain similar fungal hyphae filaments, after even relatively short periods of storage under non-sterile conditions. These microbial features may have possibly been introduced after drilling.

#### 5.4.2 Post-experimental material – Biotic Experiment (with denitrifying bacteria)

Observation of the core plug recovered after the biotic experiment, inoculated with denitrifying bacteria (*P. denitrificans*), showed that there was small channel between the core and the heat-shrunk Teflon sheath, where a small fragment of one fracture wall had fallen away and was missing (Plate 9). This extended for 15-20 mm along the interface between the core plug and the Teflon sheath but did not continue for the whole length of the plug. Thus, this may represent a partial localised pathway for some fluid movement during the course of the experiment. Close examination of the surface of this “channel” feature showed that fine-grained mineral particles were “clotted” and bound together on the surface of the fracture by a gelatinous organic film (Plate 10).

On opening along the fracture plane, the fracture surfaces were seen to have a similar “ridge-and-furrow” surface morphology to that seen in the off-cut of the starting material (Plate 11). This indicates that these potential slickenside channels were extensively present across the whole of the fracture surface throughout the core sample.

Detailed cryoSEM observations show that, as in the starting material, the fracture surface is coated with organic biofilaments (Plate 12). These form a dendritic meshwork across the fracture surface, and again, they follow and penetrate along the “channels” presented by the “ridge-and-furrow” morphological structures in the rock surface.



**Plate 9 Binocular microscope photomicrograph showing annulus channel in the outer wall of the core plug where a fragment of the opposing fracture wall has fallen away. Post-experimental material. (Biotic experiment).**

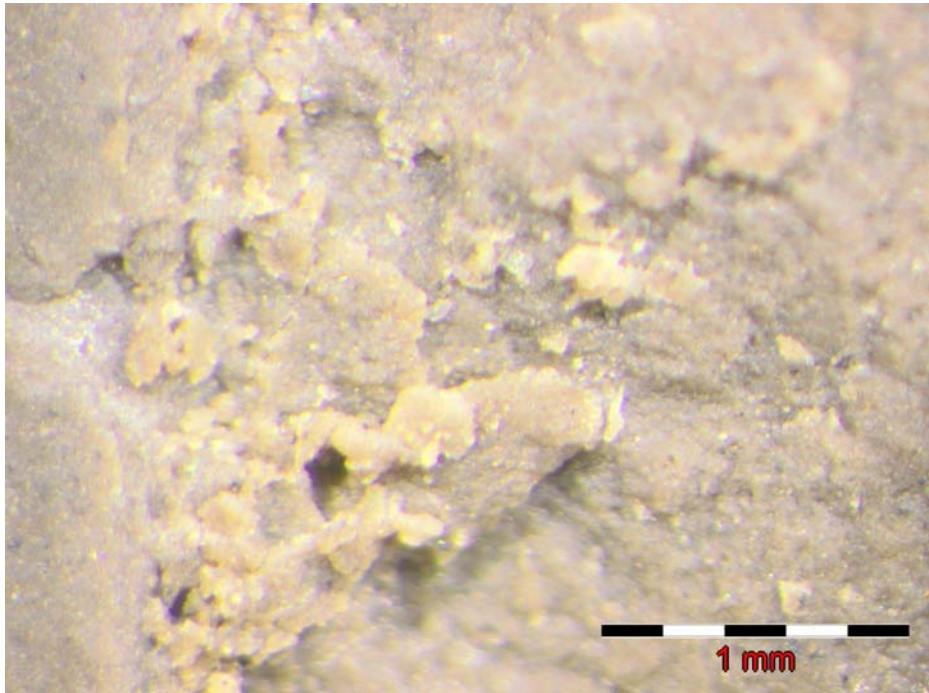


**Plate 10 Binocular microscope photomicrograph showing surface of the annulus channel in the outer wall of the core plug where a fragment of the opposing fracture wall has fallen away. Loose mineral fines are bonded to the surface by a gelatinous organic film. Post-experimental material. (Biotic experiment).**

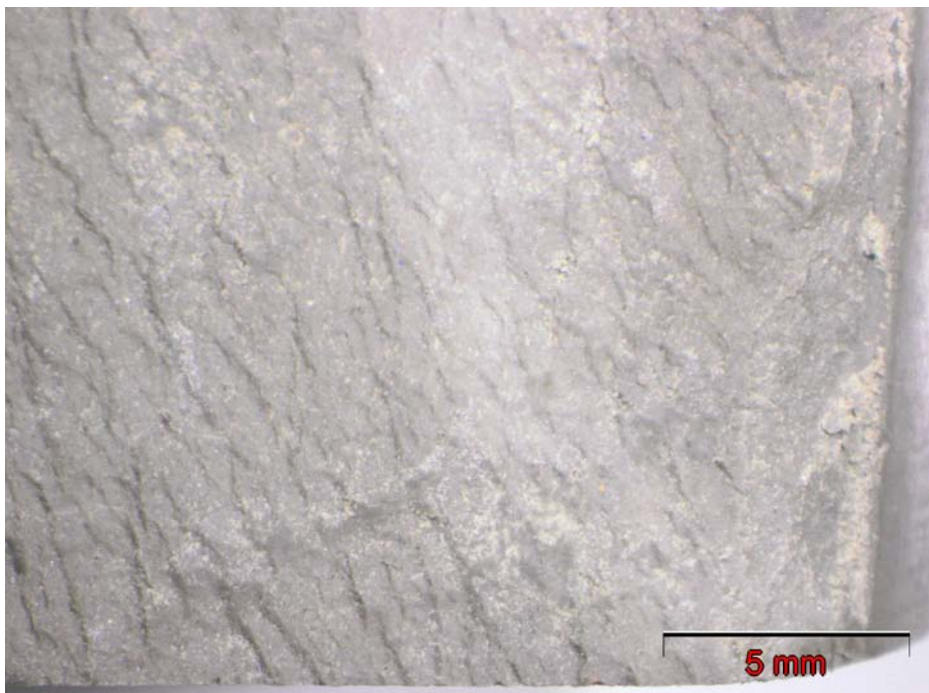


**Plate 11 Binocular microscope photomicrograph of the fracture surface showing the “ridge-and-furrow” features formed by slickensiding, and representing a network of fine microporous channels along the plane of the fracture. Post-experimental material. (Biotic experiment).**

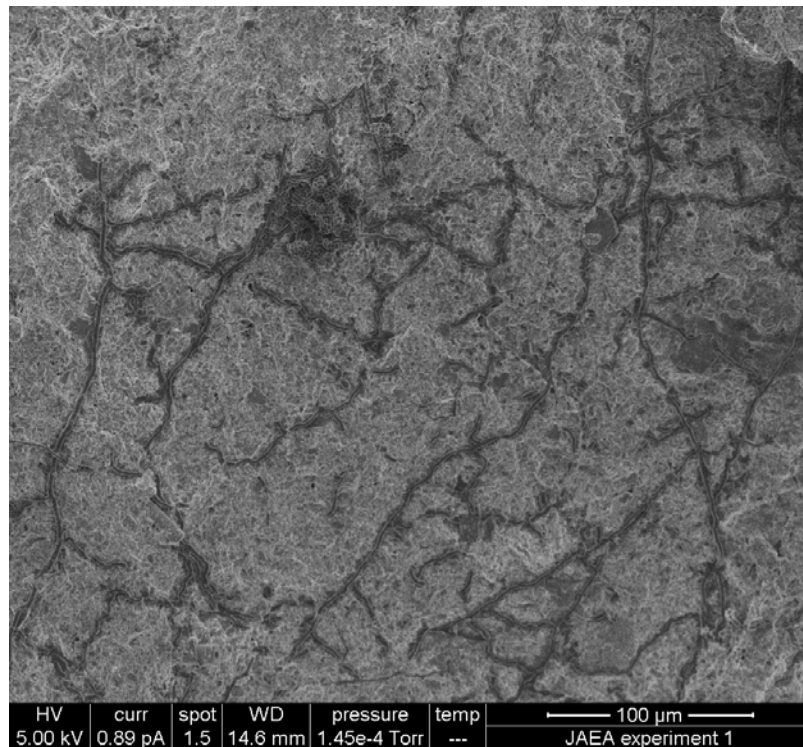


**Plate 12 CryoSEM SEI image (high vacuum cryoSEM, FEI ESEM instrument) of the fracture surface revealing a network of organic biofilaments following “ridges-and-furrows in the fracture surface. Post-experimental material. (Biotic experiment). High vacuum cryoSEM, uncoated sample, FEI ESEM instrument.**

Closer examination of the filaments suggest that many of these filaments comprise “strings” of connected “rod-like” cells that are the expected size and morphology for bacterial cells (Plate 13 and Plate 14). These cell-like structures were not observed in the starting material. However, it is not totally clear in all cases that the filaments are comprised of discrete cells, and some filaments are more similar to the filamentous structures seen in the starting material. Possibly both bacterial and fungal filaments are present.

The filamentous structures are also closely associated with isolated rod-like cells and clusters of cells (“bunches of grapes” aggregates) as seen in Plate 15 and Plate 16. Isolated rod-like cells are clearly bacterial cells and probably represent discrete cells of denitrifying bacteria. It is not clear whether the clusters of rod-like cells and the strings and filaments are related. In some cases, the rods appear to encase, and be living on, the surfaces of what appear to be possible fungal filaments (Plate 17). In other cases, the “bunches of grapes” aggregates may represent “fruiting” cells associated with parts of the filaments.

No obvious secondary mineralogical alteration products were observed on the fracture surface. The redox-sensitive minerals such as pyrite and magnesiosiderite are coated with microbial structures but show no evidence of oxidation (Plate 17 and Plate 18). However, the biofilaments do appear to have caused some etching and dissolution mineral surfaces, affecting both pyrite and silicate substrates (Plate 18 and Plate 19).

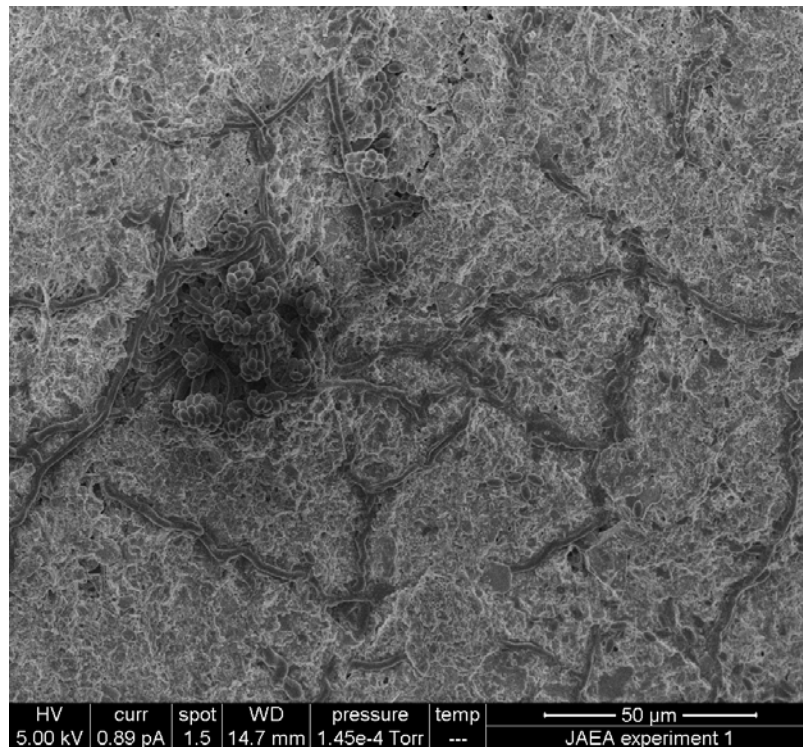


**Plate 13** CryoSEM SEI image of the fracture surface showing clusters of cellular structures associated with biofilaments and showing that some biofilaments comprise strings of rod-like cells. Post-experimental material. (Biotic experiment). High vacuum cryoSEM, uncoated sample, FEI ESEM instrument.

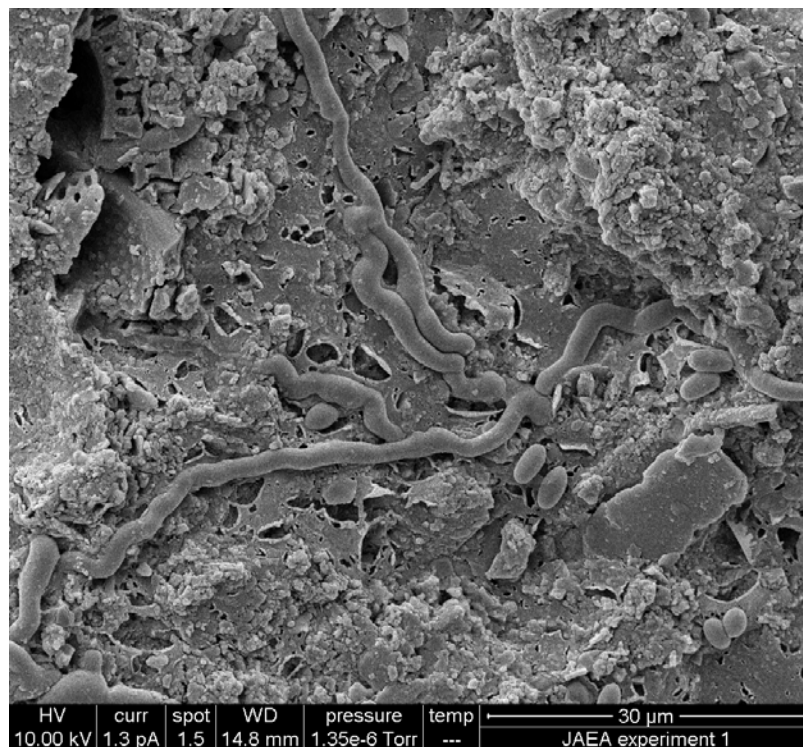


**Plate 14** CryoSEM SEI image of the fracture surface showing isolated rod-like cells associated with biofilaments that appear to comprise strings of connected rod-like cells that appear to be coated and obscured within the filament by an organic biofilm forming a sheath to the filament. Post-experimental material. (Biotic experiment). High vacuum cryoSEM, gold-coated sample, FEI ESEM instrument.

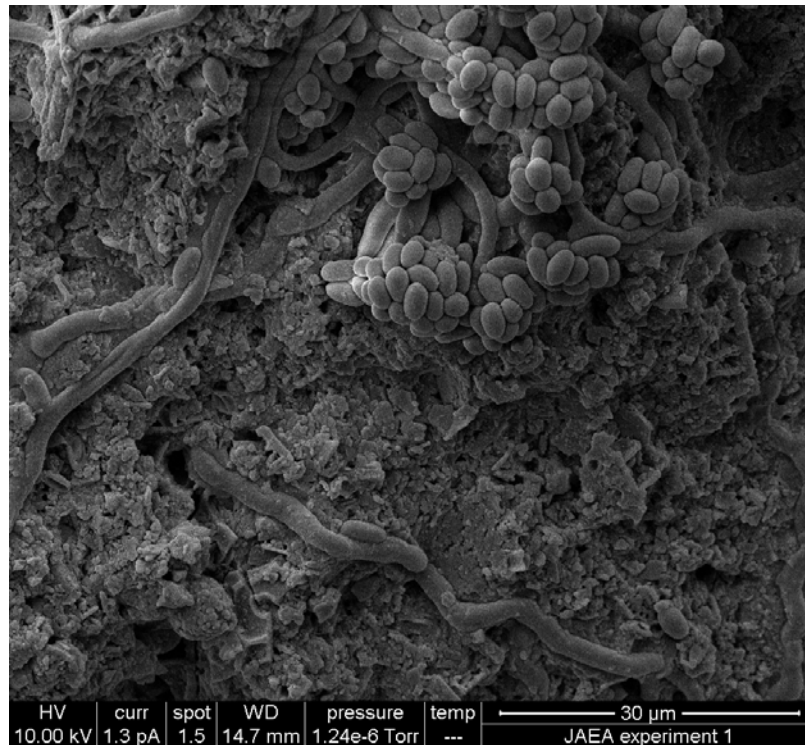


**Plate 15 CryoSEM SEI image of the fracture surface showing clusters of rod-like cells associated with biofilaments that appear to comprise strings of connected rod-like cells that appear to be coated and obscured within the filament by an organic biofilm forming a sheath to the filament. Post-experimental material. (Biotic experiment). High vacuum cryoSEM, gold-coated sample, FEI ESEM instrument.**

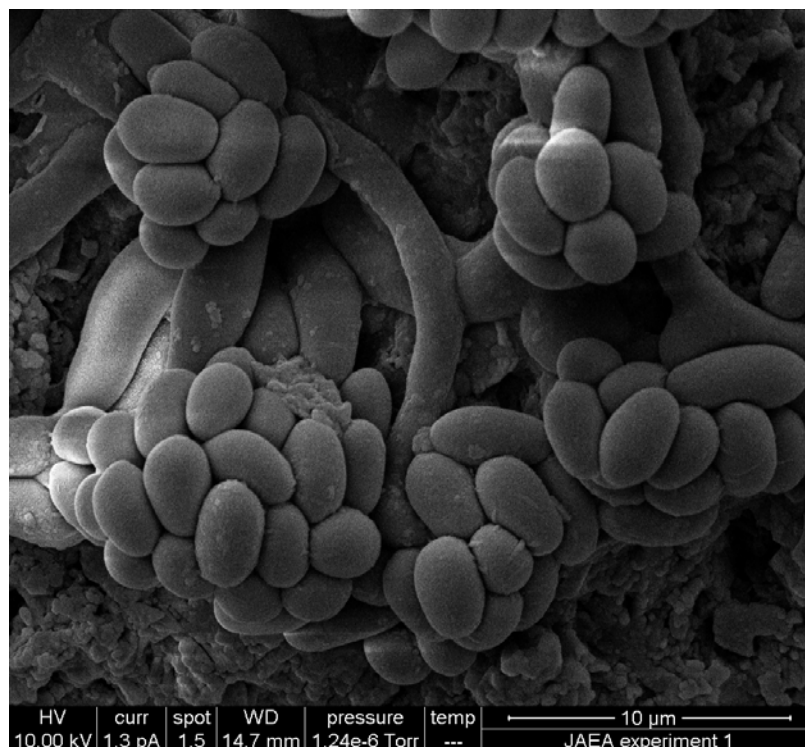


**Plate 16 CryoSEM SEI image of the fracture surface showing detail of clusters of rod-like cells associated with biofilaments. Post-experimental material (Biotic Experiment). High vacuum cryoSEM, uncoated sample, FEI ESEM instrument.**

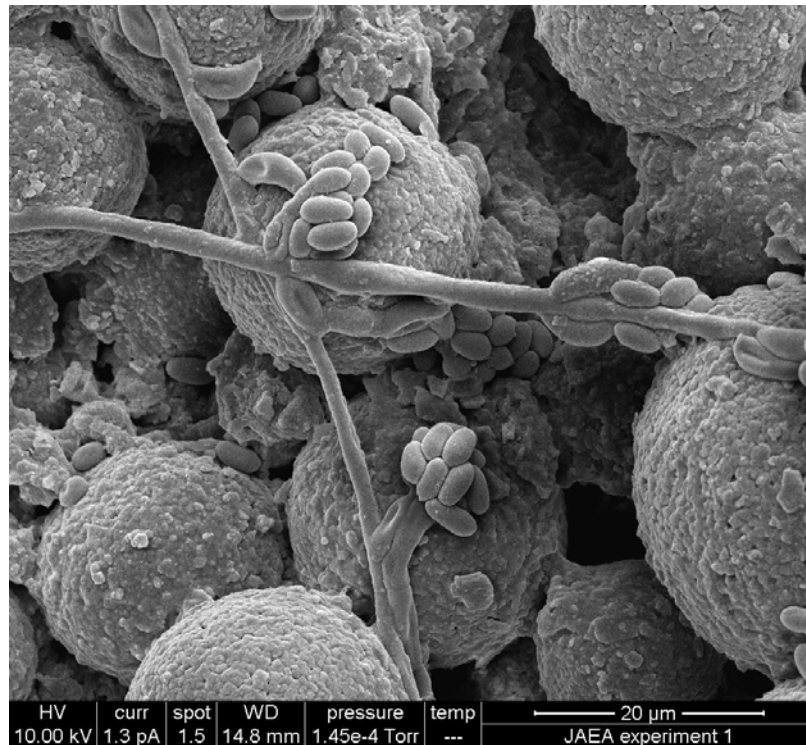


**Plate 17 CryoSEM SEI image showing clusters rod-like cells associated with biofilaments resting on fresh framboidal pyrite. Post-experimental material. (Biotic experiment). High vacuum cryoSEM, gold coated sample, FEI ESEM instrument.**

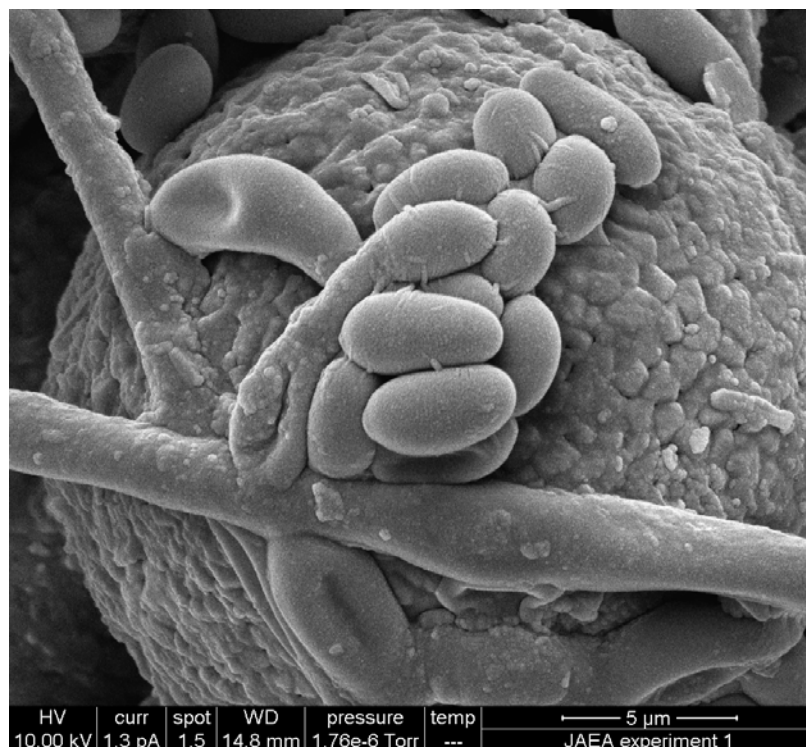


**Plate 18 CryoSEM SEI image showing detail of the clusters rod-like cells associated with biofilaments resting on fresh framboidal pyrite. Fine pili structures can be seen on the rod-like cells that may function to bind the cell to mineral surfaces and adjacent cells. The pyrite appears to be unaffected by oxidation but the biofilaments can be seen to have etched into and are now embedded in the pyrite surface. Post-experimental material. (Biotic experiment). High vacuum cryoSEM, gold coated sample, FEI ESEM instrument.**

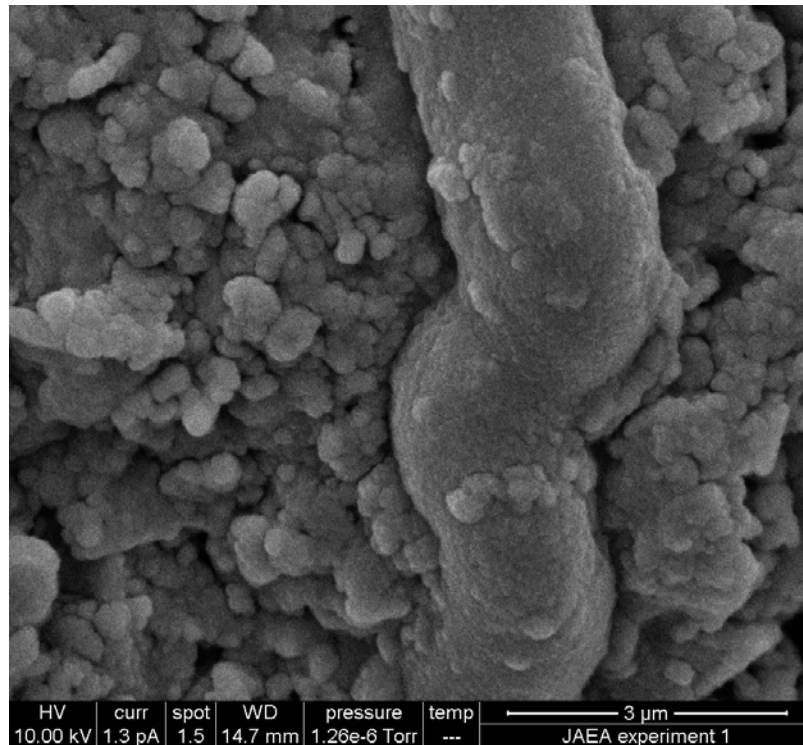


**Plate 19 CryoSEM SEI image showing a biofilaments that can be seen to have etched into and is now embedded in the siliceous sedimentary rock surface. Post-experimental material (Biotic experiment). High vacuum cryoSEM, gold-coated sample, FEI ESEM instrument.**

#### 5.4.3 Post-experimental material (Abiotic control experiment)

Observation of the core plug recovered after abiotic control experiment showed that there was channel between the core and the heat-shrunk Teflon sheath, developed along the intersection of the fracture and the core cylinder surface, where a small amount of one of the fracture walls had broken away and was missing (Plate 20). This extended for 32 mm along the interface between the core plug and the Teflon sheath but did not continue for the whole length of the plug. Thus, this may represent a partial localised pathway for some fluid movement during the course of the experiment. Closer examination of the core using binocular microscopy shows that the channel in the wall of the core plug has formed where a second lower angle fracture intersects with the principle steeply inclined fracture (Plate 21). Close examination shows that this lower angle fracture actually consists of several close-spaced, sub-parallel to anastomosing hairline fractures (<50 μm apertures) confined within a narrow zone about 8 mm wide. The fracture wall at the intersection of these two principal fracture orientations has partially brecciated and fragments of this broken wallrock have fallen away during core plug preparation to leave this channel along part of the core wall. Fracture porosity exists between the fragmented material within the steep fracture. These fractures are potential flow pathways through the core sample and these intersecting fractures represent a more complex network than was encountered in the core plug used in the biotic experiment or the unreacted comparison sample.

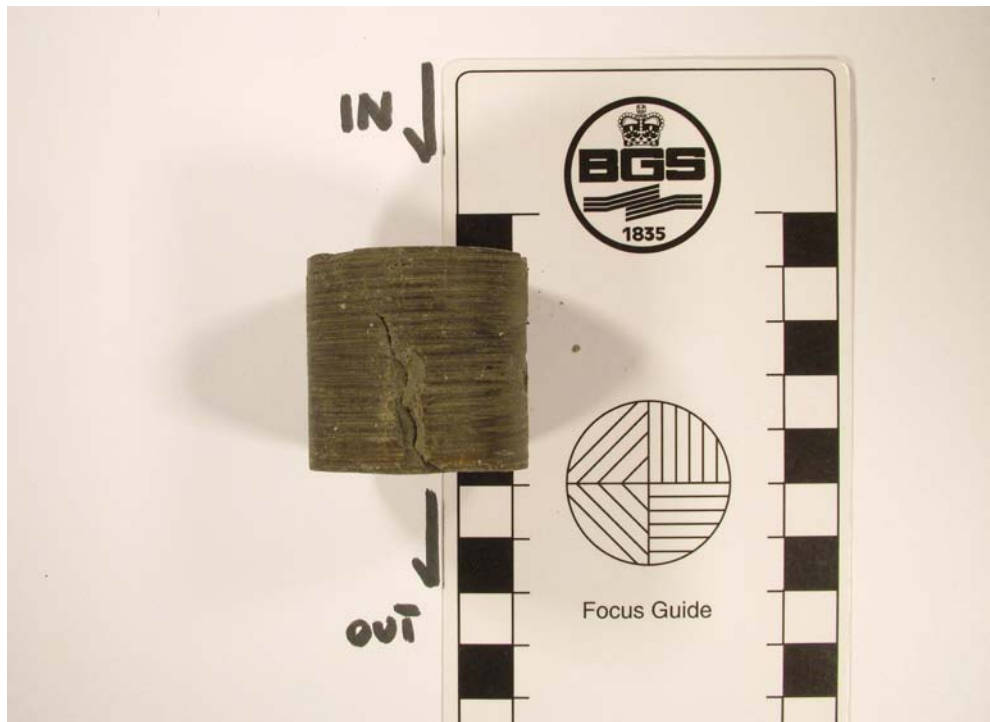


**Plate 20 Macro photograph of the reacted core plug directly after recovery from the a(Biotic experiment). A steep (70-80° dipping) fracture can be clearly seen. The trace of a second lower-angle (c.30° dipping) fracture can be seen as a dark trace on the core wall. The core has a small channel along the intersection between the fracture plane and the core cylinder wall, formed where a small amount of one fracture wall has broken away. Direction of fluid flow is shown. (Abiotic control experiment).**

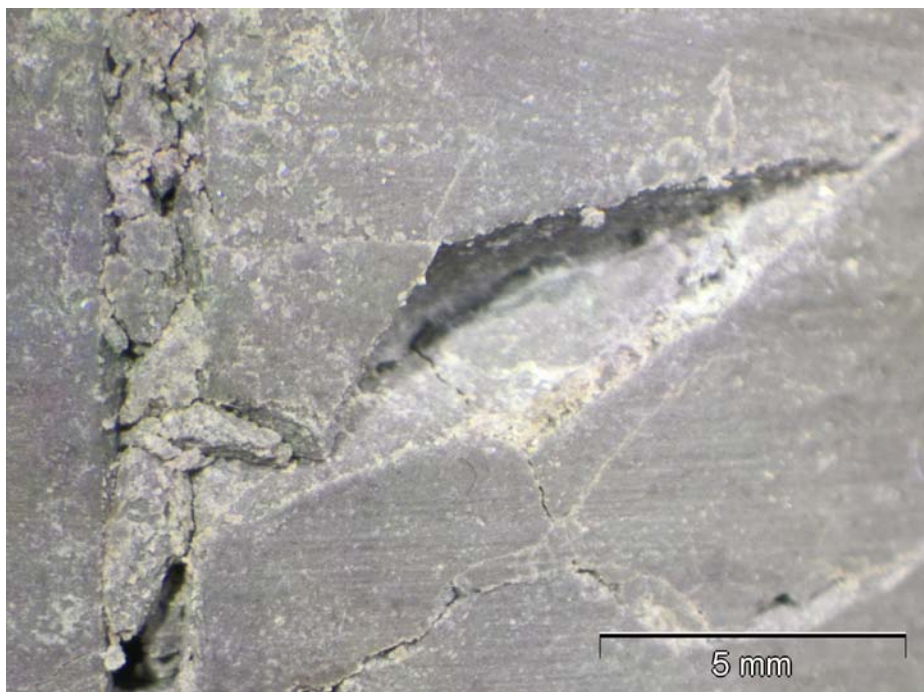


**Plate 21 Binocular microscope photomicrograph showing detail of the annulus channel in the outer wall of the core plug where a second lower angle fracture intersects with the principal steeply inclined fracture. The fracture wall at the intersection of these fractures has partially brecciated and fragments of this broken wallrock have fallen away during core plug preparation to leave this channel along part of the core wall. Fracture porosity exists between the fragmented material within the steep fracture. Post-experimental material. (Abiotic control experiment).**

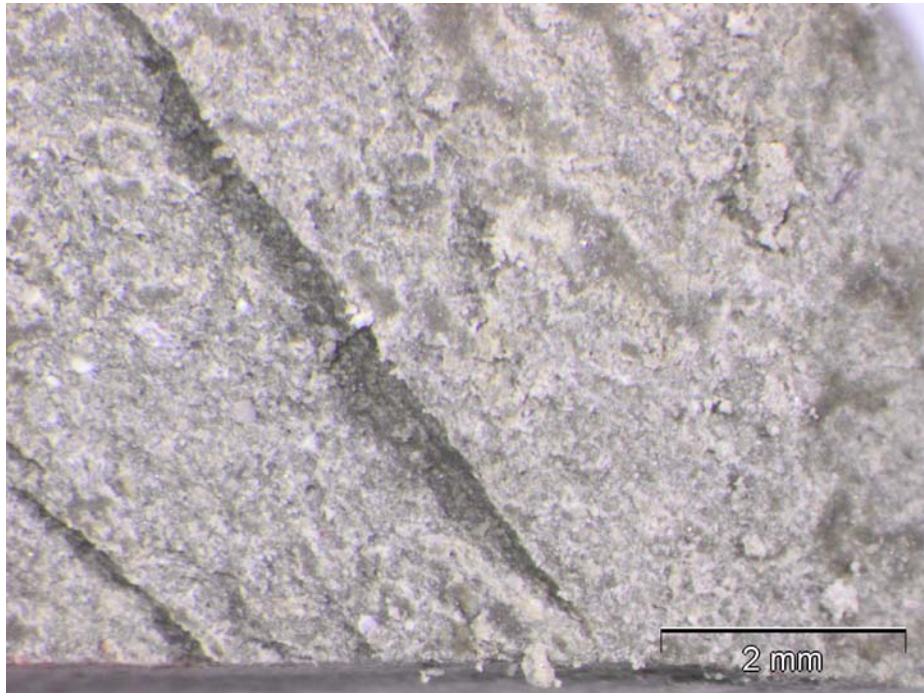


**Plate 22 Binocular microscope photomicrograph showing detail of the surface of the main steep fracture. The fracture surface exhibits a series of ridges and furrows where the surface is intersected by lower angle hairline microfractures. These asperities in the fracture surface probably produce channelled flow. Post-experimental material. (Abiotic experiment).**

The surface of the main fracture was observed to be obliquely traversed by a series of fine sub-parallel lineaments (Plate 22). These features are formed by the intersection of a series of hairline lower-angle fractures with the main fracture plane. This has produced a network of sub-parallel “ridges” and “furrows” in the main fracture surface, and these probably channel fluid flow through the fracture.

Detailed ESEM and VPSEM observations of the fracture surfaces found no evidence of any filamentous or other organic or biogenic structures similar to those found in the starting material (Section 5.4.1) and in the biotic experiment (Section 5.4.2). The surfaces of the fractures simply expose the hostrock mineralogy (Plate 23). Mineralogically, the fracture surfaces are similar to those described from the starting material and the biotic experiment. The fracture surface mineralogy is dominated by biogenic silica derived from abundant fragments of siliceous diatoms skeletons and sponge spicules (Plate 24 and Plate 25), with subordinate to minor clay minerals. The structure of the diatoms is extremely well-preserved and shows no evidence of alteration or dissolution during the experiment (Plate 24). Abundant authigenic pyrite is also present in the fracture surface, occurring as framboidal aggregates (Plate 24 and Plate 26), disseminated and clusters of coarser octahedral crystals of authigenic pyrite, and fine pyrite partially replacing diatomaceous skeletons (Plate 27) and detrital coalified woody plant fragments. Siderite is also present. Petrographical observations found no evidence for any mineralogical alteration: the authigenic pyrite and siderite are fresh with no evidence of oxidation and there is no evidence of dissolution or alteration of the siliceous and clay-rich matrix of the rock. No evidence was observed for the formation of any secondary mineral formation on the fracture surfaces.

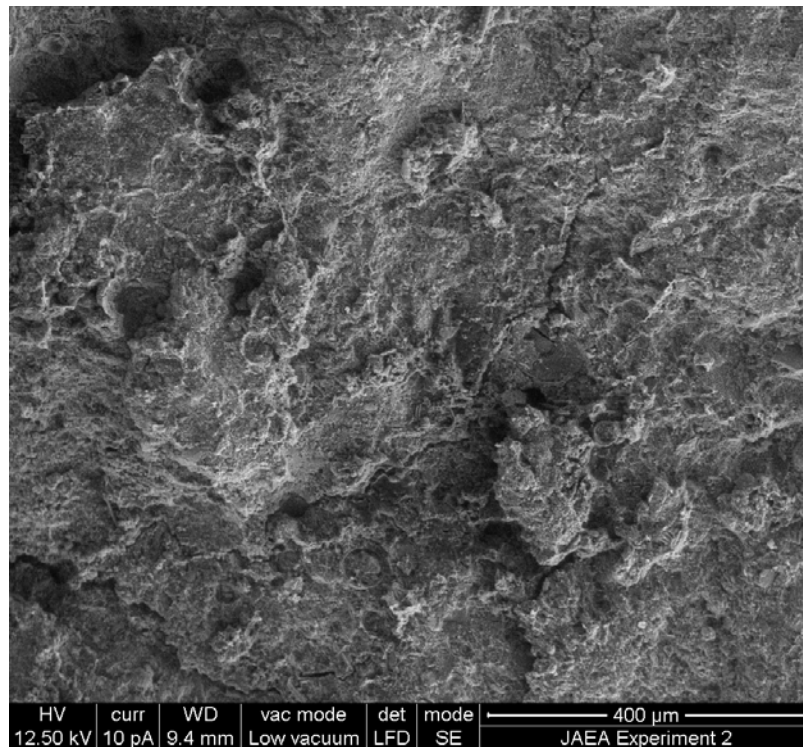


**Plate 23 ESEM SEI image showing typical rough fracture wallrock surface devoid of any microbiological features. Post-experimental material. (Abiotic experiment). ESEM uncoated sample, FEI ESEM instrument.**

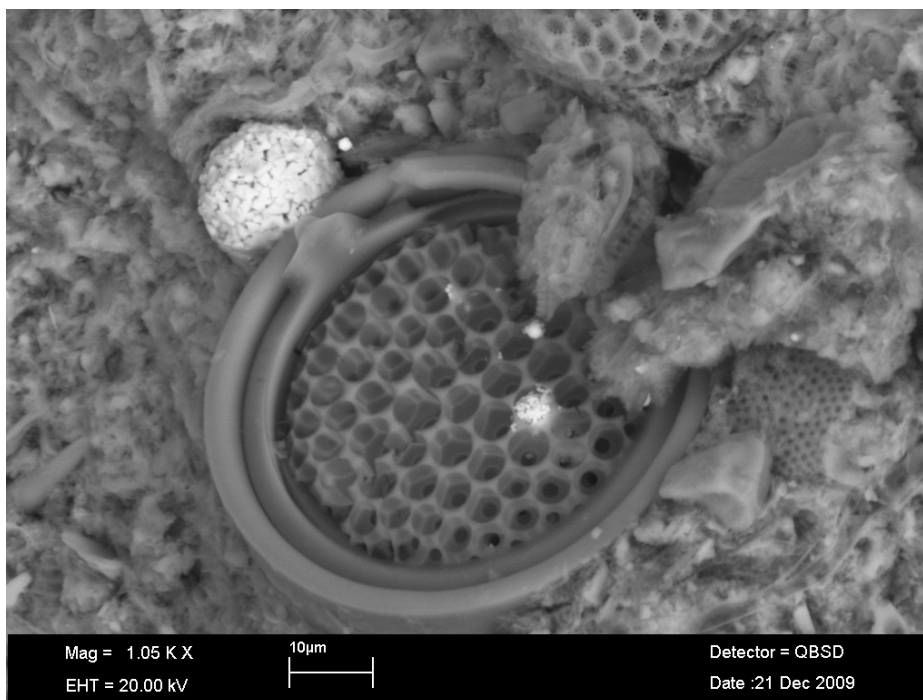


**Plate 24 BSEM image of fracture wallrock showing fabric dominated by well-preserved silica diatom structures material and fine grained silica matrix comprised of finely comminuted diatomaceous debris. Well preserved diagenetic pyrite can be seen as framboidal aggregates and as fine pyrite locally replacing the diatom structures. Post-experimental material. (Abiotic experiment). VPSEM uncoated sample, LEO 435VP SEM instrument.**

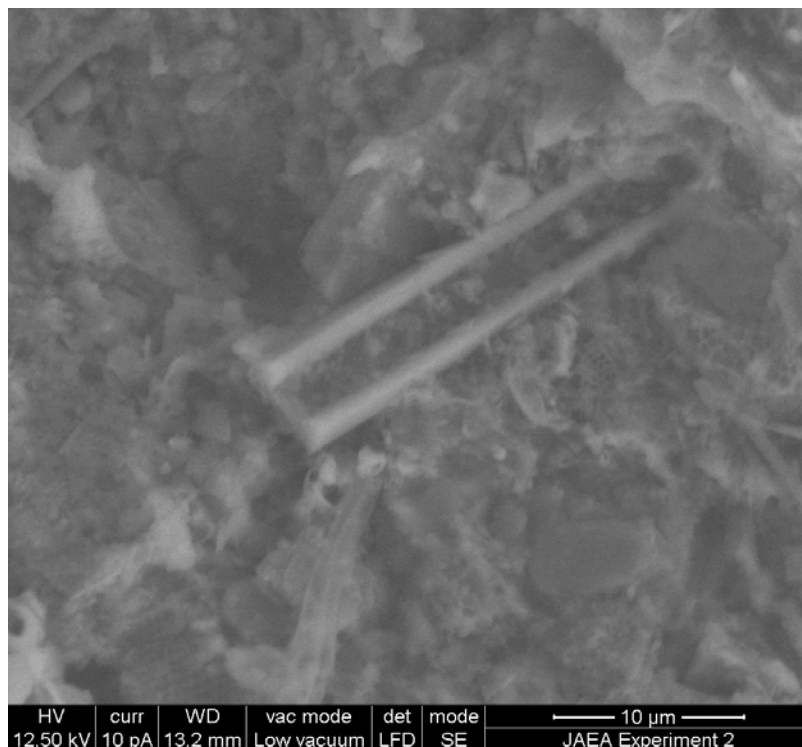


**Plate 25 ESEM SEI image showing fracture surface composed of fine fragmented biogenic silica derived from sponge spicules and siliceous diatom skeletons. Post-experimental material. (Abiotic experiment). ESEM uncoated sample, FEI ESEM instrument.**

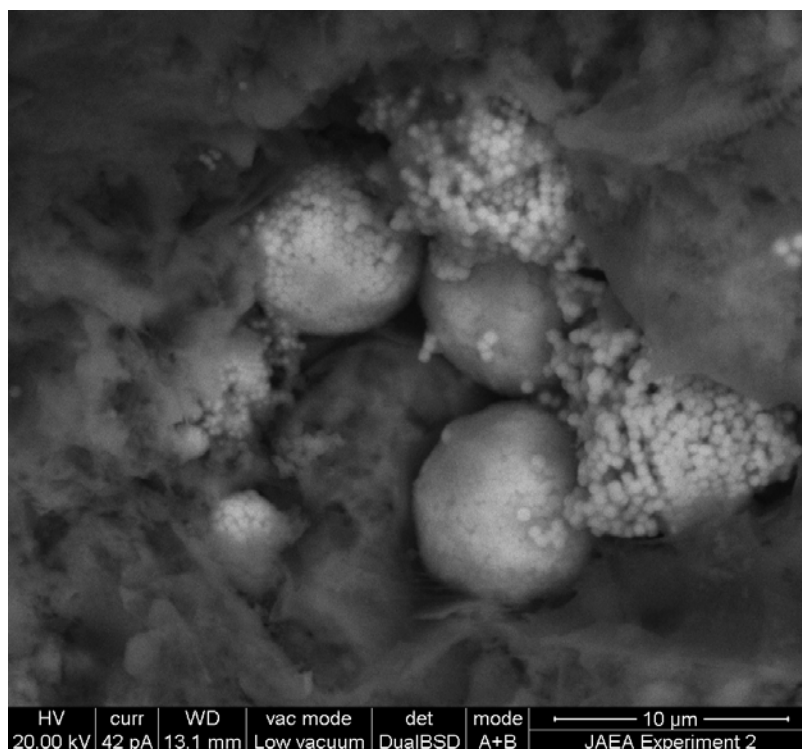


**Plate 26 ESEM SEI image showing well-preserved framboidal aggregates of authigenic pyrite exposed in the fracture surface. Post-experimental material. (Abiotic experiment). ESEM uncoated sample, FEI ESEM instrument.**

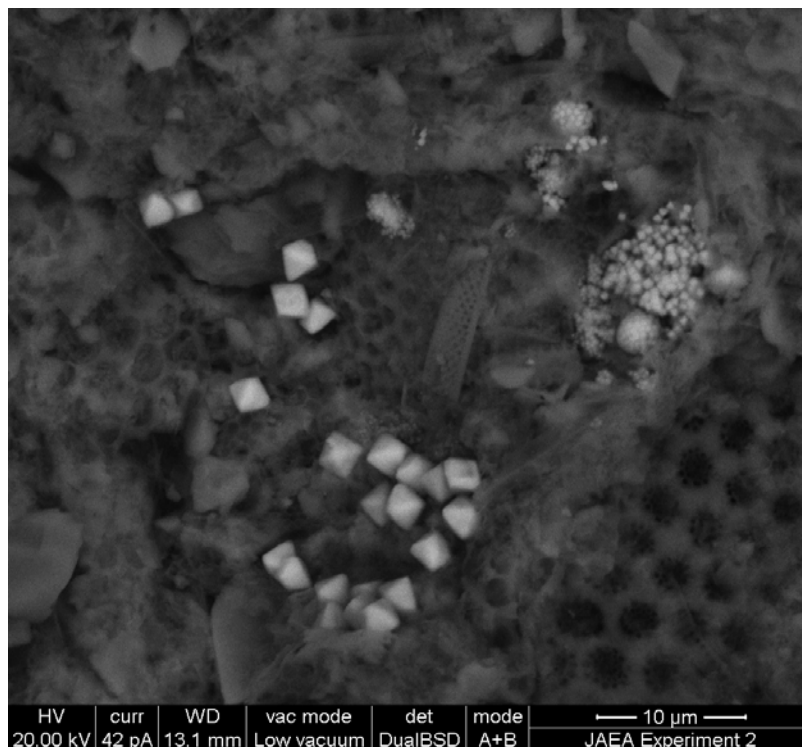


**Plate 27 ESEM SEI image showing well-preserved octahedral microcrystals of authigenic pyrite exposed in the fracture surface. The matrix of the rock comprises abundant fine silt-grade silica diatom detritus. Post-experimental material. (Abiotic experiment). ESEM uncoated sample, FEI ESEM instrument.**

## 6 Discussion

Both the biotic and abiotic column experiments were pilot studies of short duration (39 days maximum) although injection of bacteria into the biotic column experiment took place only over a period of 28 days. Nevertheless, the results show that *P. denitrificans* can survive under pressurised conditions for this period. Bacterial total numbers appear to increase from  $1.18 \times 10^5$  ( $8.88 \times 10^3$  SE) bacteria  $\text{ml}^{-1}$  on injection to  $4.48 \times 10^5$  ( $7.07 \times 10^4$  SE) bacteria  $\text{ml}^{-1}$  in the outflow fluid indicating that conditions are conducive to the growth and activity of this organism.

There were very few changes in the fluid chemistry for both the biotic and abiotic column experiments. This was due to the short duration of these pilot studies. However, chemical analysis showed that the concentrations of organic carbon (NPOC) varied greatly in the Horonobe core material.

Biological material was observed in the starting material and in post-experimental biotic material but not from post-experimental abiotic material. The structures observed in the biotic column experiment were significantly morphologically different to those seen in the starting material. Although it might be considered that some morphological differences could be attributed to differences in sample preparation – the starting material was examined as air-dried material and could have collapsed due to dehydration, whereas the biotic experiment material was examined in a moist or water-saturated state. However, there were clear morphological differences between the biogenic features seen in the starting material and the biotic experiment. The biogenic features seen in the biotic experiment included obvious clusters of cellular structures, isolated cells, and strings of cells of similar size to that expected for bacteria. Furthermore, these cells exhibited fine pili structures that are consistent with certain bacterial structures. In contrast, only fine organic filaments with no cellular structures were observed in the starting material.

Filaments were also seen covering the fracture surface after completion of biotic column experiment. These filaments appeared to be different to those observed in the starting material. In many cases, the biotic column experiment biogenic filaments were closely associated with clusters of microbial cellular structures. In addition, some filaments appeared to consist of “strings” of elongate cells enclosed in an organic film or mucilage, whereas this was not seen in the starting material. Finally, these filaments from the biotic experiment were observed to have locally etched the mineral substrate, and again this was not seen in the starting material. Similar biofilaments have been observed in other flow-through column experiments examining biofilm impacts on fluid transport through crushed diorite but under unpressurised conditions (Hama *et al.*, 2001; Tuck *et al.*, 2006; Coombs *et al.*, 2008).

Therefore, it can be concluded that although the starting material had been affected by the activity of microbial contamination, this was completely different to the microbial effects seen in biotic column experiment. We interpret the microbial structures observed in the starting material as probable fungal filaments, produced by fungal degradation of the core samples after the cores were drilled. Potential microbiological contamination of sampled core is well recognised (e.g. Stroes-Gascoyne and West, 1996; Chapelle, 2000; Stroes-Gascoyne *et al.*, 2007; Hallbeck and Pedersen, 2008; Polson *et al.*, 2010) and the current study further illustrates this fact. However, the markedly different biological structures observed in the post-experimental biotic material were interpreted as a filamentous biofilm resulting from the activity of *P. denitrificans* introduced during the experiment. These filaments have utilised small microscopic channels in the fracture plane where tiny sub-parallel “ridges” and “troughs” formed as a result of shear along the fracture (i.e. slickensides) which create surface irregularities (or asperities) that do not fully interlock because of tiny displacement along the fracture surface. These represent potential fluid flow paths along the fracture. Similar microscopic channel like fluid transport pathways were also exploited by the growth of fungal contamination in the contaminated starting material.

Petrographical observations found no evidence for the oxidation of neither pyrite nor siderite in either the biotic experiment or the abiotic column experiment. In both cases, the pyrite surfaces were found to be fresh and free from any secondary iron oxide formation. In the biotic column experiment however, it was found that the microbial filaments had etched into the underlying rock substrate. The etching appeared to be non-specific with regard to surface mineralogy, affecting the silica-rich matrix, pyrite and siderite. No alteration or dissolution effects were observed in the starting material or in the abiotic column experiment. The interactions of microbes and minerals is long recognised (e.g. Beveridge *et al.*, 1997; Ehrlich 1999; Konhauser *et al.*, 1998; Milodowski *et al.*, 1990; Tuck *et al.*, 2006; Konhauser 2007) and past work has extensively demonstrated microbial dissolution of iron minerals such as pyrite and haematite, manganese and arsenic-bearing minerals and clay minerals (Southam and Saunders 2005; Konhauser 2007; Shock, 2009). The current observations show that microbial etching of minerals in mudstones can also take place under pressurised conditions.

Fluctuations in pressure within the cores were detected by the transducers during the biotic and abiotic column experiments. The pressure profile of the abiotic column showed small changes in permeability which could be the result of partial blocking of pore spaces by fines and the subsequent flushing of material as new pathways were established. Overall, the pressure profile for the biotic column experiment followed a similar pattern to the flux observed in the abiotic column; however sharp ‘spikes’ were observed in the data between 23 and 30 days from the start of the biotic experiment. This feature could not be attributed to transducer noise as quiescent periods in the data were bracketed by pressure maxima and minima spanning time periods of several hours. As these sudden changes in pressure were only observed in the biotic column experiment, it was probably due to the formation of the observed biofilm. Previous unpressurised flow-through experiments with crushed diorite have also showed that biofilms influenced fluid flow (Hama *et al.*, 2001; Tuck *et al.*, 2006; Coombs *et al.*, 2008).

## 7 Conclusions

The results from these experiments provide some insights into the influences of biofilms on fracture surfaces. These can be summarised as:

- **Biological material was observed in the starting material and in material from the completed biotic experiment** but not from material from the completed abiotic experiment. The starting material appeared to be contaminated with fungal hyphae which occurred prior to its arrival at BGS. The observed biological material arising from the biotic experiments are different in nature and we attribute this to the activity of *P. denitrificans* during the experiment.
- Both the biotic and abiotic control experiments were of very short duration with injection of bacteria in the biotic experiment only over a period of 28 days. The results show that *P. denitrificans* can survive in the core material over this period and that total numbers appear to increase in the outflow fluid indicating that the environment within the core is conducive to the growth and activity of this organism. Clearly, ***P. denitrificans* can survive and thrive in the pressurised flow through column experiments** containing fractured material from Horonobe (flow rate of  $300 \mu\text{l hr}^{-1}$ ) when exposed to synthetic Horonobe groundwater (supplemented with sodium acetate at  $0.2500 \text{ g l}^{-1}$  at JAEA's request) over a period of 28 days.
- Organic filaments covered the fracture surface from the biotic experiment together with *P. denitrificans* cells. **Thus a biofilm had formed in the columns injected with *P. denitrificans* although, given the short duration of the experiment, the biofilm was poorly formed.** These filaments appeared to be different to those observed in the starting material with clusters of microbial cellular structures present. In addition, some filaments appeared to consist of "strings" of elongate cells enclosed in an organic film or mucilage, whereas this was not seen in the starting material.
- **The features observed in the biotic experiment suggest that the bacteria produced filamentous biofilms** These filaments have utilised small microscopic channels in the fracture plane where tiny sub-parallel "ridges" and "troughs" formed as a result of shear along the fracture (i.e. slickensides) which create surface irregularities (or asperities) that do not fully interlock because of tiny displacement along the fracture surface. These represent potential fluid flow paths along the fracture. Similar microscopic channel-like fluid transport pathways were also exploited by the growth of fungi in the contaminated starting material.
- There was no petrographical evidence for the oxidation of pyrite or siderite in either the biotic experiment or the abiotic control experiment. However, **in the biotic experiment, the bacterial filaments had etched into the underlying rock substrate. The etching appeared to be non-specific with regard to surface mineralogy, affecting the silica-rich matrix, pyrite and siderite.** No alteration or dissolution effects were observed in the starting material or in the abiotic control experiment.
- Essentially, **there were very few changes in the fluid chemistry for both the biotic and abiotic experiments.** No significant differences were observed the chemistry of the outflow fluid from the biotic column when compared to the abiotic column. This implies that the duration of each test may not have been long enough to allow chemical changes to be observed.
- **Fluctuations in pressure profiles of the cores were detected by the transducers during the experiments.** Overall, the changes in pressure could be explained by partial clogging of conductive pathways which were then flushed as the hydraulic pressure locally increased. The resultant rapid saw-tooth like pressure profile

observed in the biotic core during the experiment was symptomatic of a dynamic system exhibiting localised intermittent changes in permeability. However, the changes in pressure observed in the abiotic column were more likely to be the result of slow changes in flow geometry within the core giving rise to an overall change in permeability. Since the distinctive 'spikes' observed in the pressure graph of the biotic core material were not seen in the abiotic experiment, they may only be explained by the observed biofilm formation.

## 8 Recommendations

These short pilot studies have shown for the first time that *Pseudomonas denitrificans* can survive and thrive when injected into flow-through column experiments containing diatomaceous mudstone material (Keotoi formation from Horonobe, Japan) and synthetic groundwater, supplemented with sodium acetate, under pressurised conditions. The experiments also demonstrate that it is possible to study microbially mediated changes in fractured cores using this technique. These same methodologies could also be adapted to obtain information from core from a variety of geological environments including oil reservoirs, aquifers and waste disposal sites to provide an understanding of the impact of microbial activity on the transport of a range of solutes, such as groundwater contaminants and gases (e.g. injected carbon dioxide).

These pilot column experiments have generated a number of further questions and uncertainties. Although there were few significant changes in the fluid chemistry, changes in the permeability of the core material in the columns were quantitatively monitored and the pressure profiles of the cores seem to indicate that microbial activity contributes to changes in fluid flow once biofilaments are established in the pore spaces. These pressure profiles are indicative of the material achieving a number of apparent quasi-steady states, suggesting highly dynamic and evolving systems. However, since the experiments were of very short duration, there was little time for extensive biofilm development. Nevertheless, the observations from the experiments have shown that biofilms from *P. denitrificans* do form over 28 days and that physical etching of minerals by biological material is occurring. Additionally, an effective methodology has now been developed to gain robust data in any future experiments.

Minimal chemical information has been generated from these short-term column experiments which can be used in a computer model (Tochigi *et al.*, 2007). Longer duration experiments (i.e. over a period of a year or more) are needed to obtain such data which would also yield information on the impacts of biofilms on fracture transport properties which is of great significance in understanding fluid movement in and around a repository. Long-term experiments will also allow equilibration of the experimental systems prior to injection of the perturbing organisms.

## Appendix 1 Groundwater composition

Chemical composition of groundwater (mg l<sup>-1</sup>) from borehole HDB-10 (2008)

Temperature (°C)		31.0
ORP (mV)	9	-250
pH		6.25
B	(mg/l)	136
Ca	(mg/l)	105
Fe	(mg/l)	< 0.1
Total Fe <sup>(a)</sup>	(mg/l)	2.74
Fe <sup>2+</sup> <sup>(a)</sup>	(mg/l)	2.74
Mg	(mg/l)	110
Si	(mg/l)	24.8
Mn	(mg/l)	< 0.1
Mn <sup>(a)</sup>	(mg/l)	0.065
K	(mg/l)	129
Na	(mg/l)	4930
F <sup>-</sup>	(mg/l)	< 1
Cl <sup>-</sup>	(mg/l)	7300
NO <sub>2</sub> <sup>-</sup>	(mg/l)	< 20
Br <sup>-</sup>	(mg/l)	76
NO <sub>3</sub> <sup>-</sup>	(mg/l)	< 2
PO <sub>4</sub> <sup>3-</sup>	(mg/l)	< 5
SO <sub>4</sub> <sup>2-</sup>	(mg/l)	< 2
Total sulphide <sup>(a)</sup>	(mg/l)	24.5
NH <sub>4</sub>	(mg/l)	220
TOC	(mg/l)	22
IC	(mg/l)	590
H <sub>2</sub> CO <sub>3</sub>	(mg/l)	717
HCO <sub>3</sub> <sup>-</sup>	(mg/l)	2290
CO <sub>3</sub> <sup>2-</sup>	(mg/l)	1

<sup>a</sup> analysis with Hach-DR 2800 Portable Spectrophotometer.

## Appendix 2 Fluid chemistry

LIMS Code	Sample ID	Time Elapsed Day	pH	Ca <sup>2+</sup> mg l <sup>-1</sup>	Mg <sup>2+</sup> mg l <sup>-1</sup>	Na <sup>+</sup> mg l <sup>-1</sup>	K <sup>+</sup> mg l <sup>-1</sup>	CO <sub>3</sub> <sup>2-</sup> mg l <sup>-1</sup>	HCO <sub>3</sub> <sup>-</sup> mg l <sup>-1</sup>	Cl <sup>-</sup> mg l <sup>-1</sup>	SO <sub>4</sub> <sup>2-</sup> mg l <sup>-1</sup>	NO <sub>3</sub> <sup>-</sup> mg l <sup>-1</sup>	Br <sup>-</sup> mg l <sup>-1</sup>	NO <sub>2</sub> <sup>-</sup> mg l <sup>-1</sup>	HPO <sub>4</sub> <sup>2-</sup> mg l <sup>-1</sup>	F <sup>-</sup> mg l <sup>-1</sup>
12268-0001	Fresh GW	n/a	8.19	136.6	105.2	5587.1	140.0	127.0	970.0	8202.7	<5	<2	74.2	<1	<10	<1
12268-0003	Nutrient Broth	n/a	7.26	2.70	1.51	2999.7	146.9	-	-	4269.5	28.1	2.02	<2	5.73	38.5	<1
12268-0005	Innoculant	n/a	7.65	110.3	104.4	5593.3	143.6	-	696.5	8311.0	7.02	24.2	75.6	<1	<10	<1
12268-0002	Startup Biotic	0	6.81	196.8	130.0	4160.7	225.5	-	135.8	5578.2	1940.4	2.66	47.5	<1	<10	<1
12268-0004	T1 Biotic	5	7.81	119.6	98.2	5344.0	219.3	204.0	286.0	8204.4	28.7	<2	73.6	<1	<10	<1
12268-0006	T2 Biotic	12	8.08	97.4	95.0	5447.2	191.0	166.0	755.0	8109.1	10.4	<2	73.6	<1	<10	<1
12268-0007	T3 Biotic	19	8.19	92.9	100.0	5669.5	172.9	161.0	819.0	8280.3	7.05	<2	75.0	<1	<10	<1
12268-0008	T4 Biotic	26	8.06	91.4	101.8	5532.3	161.7	148.0	878.0	8251.9	6.49	<2	73.9	<1	<10	<1
12268-0009	T5 Biotic	33	8.22	93.7	99.5	5449.9	150.3	109.0	955.0	8254.3	5.38	<2	85.7	<1	<10	<1
12296-0001	Startup Abiotic	0	5.33	405.4	261.1	4265.3	264.2	-	-	5691.5	4463.8	3.19	52.0	<1	<10	<1
12296-0002	A2 Abiotic	7	7.37	247.5	161.3	4796.4	214.4	-	167.2	7875.3	816.1	<2	75.1	<1	<10	<1
12296-0003	A3 Abiotic	15	8.05	146.2	116.8	5003.7	179.2	86.0	336.0	8199.2	137.5	<2	79.4	<1	<10	<1
12296-0004	A4 Abiotic	22	8.31	105.3	94.5	5257.8	157.6	134.0	567.0	8154.9	27.7	<2	73.9	<1	<10	<1
12296-0005	A5 Abiotic	28	8.23	95.4	88.7	5019.3	143.1	142.0	734.0	8206.3	13.4	<2	80.3	<1	<10	<1
12296-0006	A6 Abiotic	32	8.32	98.9	93.4	5249.9	146.6	151.0	766.0	8187.6	7.44	<2	79.6	<1	<10	<1

LIMS Code	Sample ID	Time Elapsed Day	NPOC mg l <sup>-1</sup>	Total P mg l <sup>-1</sup>	Total S mg l <sup>-1</sup>	Si mg l <sup>-1</sup>	SiO <sub>2</sub> mg l <sup>-1</sup>	Ba mg l <sup>-1</sup>	Sr mg l <sup>-1</sup>	Mn mg l <sup>-1</sup>	Total Fe mg l <sup>-1</sup>	Reduced Fe mg l <sup>-1</sup>
12268-0001	Fresh GW	n/a	43.1	1.32	1.16	38.7	82.8	0.028	0.023	0.274	0.177	n/d
12268-0003	Nutrient Broth	n/a	2680.0	32.7	54.1	3.07	6.56	0.009	0.008	0.016	0.196	n/d
12268-0005	Innoculant	n/a	14.9	1.12	1.57	41.7	89.3	0.008	0.088	0.178	0.163	n/d
12268-0002	Startup Biotic	0	62.5	0.011	1265.1	17.7	37.8	0.140	2.36	2.94	46.7	present
12268-0004	T1 Biotic	5	39.6	<0.01	24.0	12.8	27.4	1.09	1.67	0.659	0.202	n/d
12268-0006	T2 Biotic	12	30.5	<0.01	10.5	12.6	27.0	1.96	1.29	0.449	0.152	n/d
12268-0007	T3 Biotic	19	33.9	<0.01	6.73	12.8	27.4	1.90	0.682	0.409	0.152	n/d
12268-0008	T4 Biotic	26	30.8	<0.01	5.33	13.1	28.1	1.54	0.343	0.365	0.165	n/d
12268-0009	T5 Biotic	33	29.0	<0.01	4.17	13.1	27.9	1.25	0.172	0.319	0.156	n/d
12296-0001	Startup Abiotic	0	43.1	0.032	1913.9	29.3	62.7	0.098	3.24	10.5	121.8	present
12296-0002	A2 Abiotic	7	6370.0	0.026	414.4	16.7	35.7	0.162	1.64	4.16	24.6	present
12296-0003	A3 Abiotic	15	5028.0	0.024	80.6	13.0	27.8	0.366	1.04	1.56	0.331	n/d
12296-0004	A4 Abiotic	22	4345.0	0.012	19.8	11.8	25.2	1.11	0.798	0.430	0.161	n/d
12296-0005	A5 Abiotic	28	4178.0	<0.01	10.9	11.3	24.2	1.62	0.690	0.248	0.146	n/d
12296-0006	A6 Abiotic	32	4125.0	0.020	8.50	11.9	25.6	1.91	0.654	0.211	0.160	n/d

n/d not determined due to colorimetric interference

LIMS Code	Sample ID	Time Elapsed	Al	Co	Ni	Cu	Zn	Cr	Mo	Cd	Pb	V	Li	B	As	Se
		Day	mg l <sup>-1</sup>													
12268-0001	Fresh GW	n/a	0.127	<0.002	<0.005	<0.005	0.088	0.018	<0.015	<0.002	<0.001	<0.001	<0.025	134.9	<0.015	<0.025
12268-0003	Nutrient Broth	n/a	0.054	<0.002	<0.005	0.006	0.654	0.006	<0.015	<0.002	<0.001	<0.001	<0.025	0.165	<0.015	<0.025
12268-0005	Innoculant	n/a	0.135	<0.002	<0.005	<0.005	0.099	0.020	<0.015	<0.002	<0.001	0.025	<0.025	140.2	<0.015	<0.025
12268-0002	Startup Biotic	0	0.291	0.380	9.37	<0.005	1.59	0.766	0.072	0.004	<0.001	<0.001	7.38	109.3	0.023	0.191
12268-0004	T1 Biotic	5	0.031	0.026	1.37	<0.005	0.290	0.029	0.417	0.002	<0.001	<0.001	0.365	127.8	0.021	0.045
12268-0006	T2 Biotic	12	0.017	0.010	0.728	<0.005	0.090	0.011	0.258	<0.002	<0.001	<0.001	0.064	134.7	<0.015	<0.025
12268-0007	T3 Biotic	19	0.022	0.005	0.314	<0.005	0.067	0.010	0.106	<0.002	<0.001	0.022	0.032	135.9	<0.015	<0.025
12268-0008	T4 Biotic	26	-0.010	<0.002	0.163	<0.005	0.046	0.008	0.051	<0.002	<0.001	0.023	<0.025	137.8	<0.015	<0.025
12268-0009	T5 Biotic Startup	33	0.025	<0.002	0.115	<0.005	0.048	0.009	0.030	<0.002	<0.001	0.011	<0.025	133.0	0.017	0.037
12296-0001	Abiotic	0	0.309	1.03	10.0	<0.005	11.7	0.486	0.050	0.053	<0.001	<0.001	5.81	109.2	0.274	0.263
12296-0002	A2 Abiotic	7	0.033	0.275	2.99	<0.005	2.24	0.033	0.039	0.017	<0.001	<0.001	1.11	120.7	<0.015	0.101
12296-0003	A3 Abiotic	15	0.015	0.043	0.516	<0.005	0.301	0.016	0.046	0.007	0.022	<0.001	0.253	123.0	<0.015	<0.025
12296-0004	A4 Abiotic	22	0.019	<0.002	0.125	<0.005	0.034	0.009	0.088	<0.002	<0.001	0.015	0.057	124.0	0.030	0.037
12296-0005	A5 Abiotic	28	0.022	-0.002	0.053	<0.005	0.018	0.010	0.090	<0.002	<0.001	<0.001	0.030	129.0	0.048	<0.025
12296-0006	A6 Abiotic	32	0.028	<0.002	0.077	<0.005	0.034	0.008	0.089	<0.002	0.021	0.022	<0.025	133.7	<0.015	<0.025

## Appendix 3 X-ray diffraction traces

### KEY

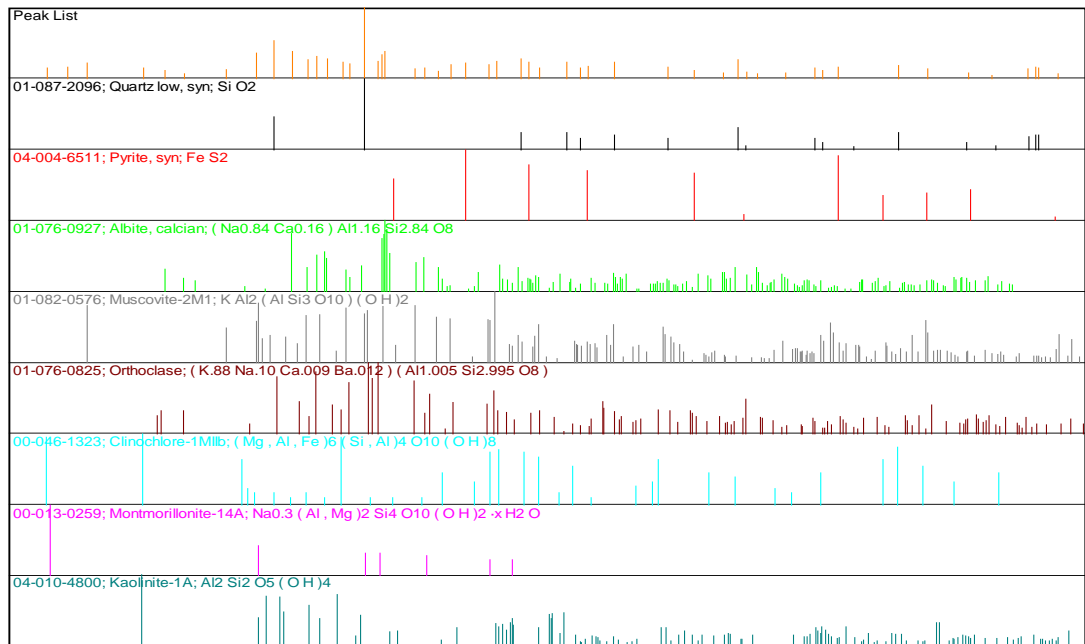
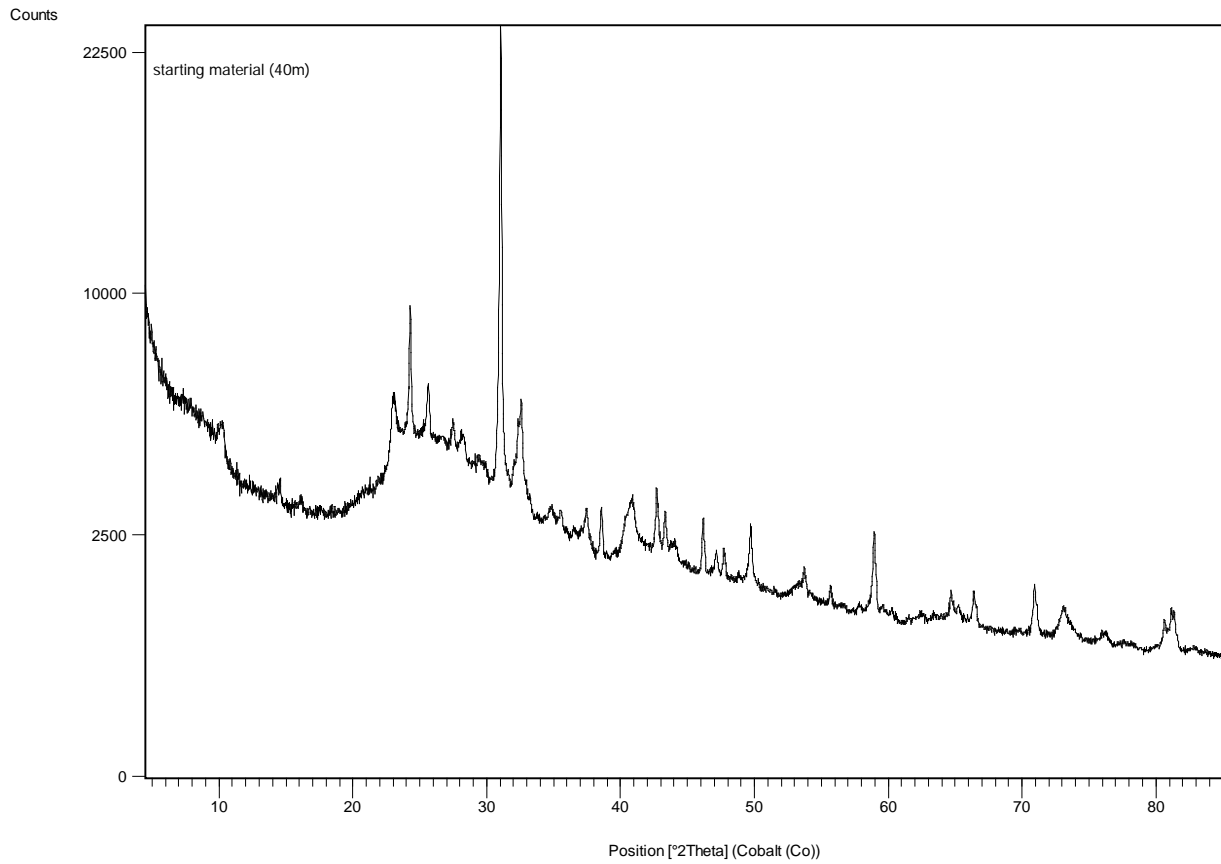
Vertical axis – Intensity (counts per second)

Horizontal axis -  $^{\circ}2\theta$  Cu-K $\alpha$

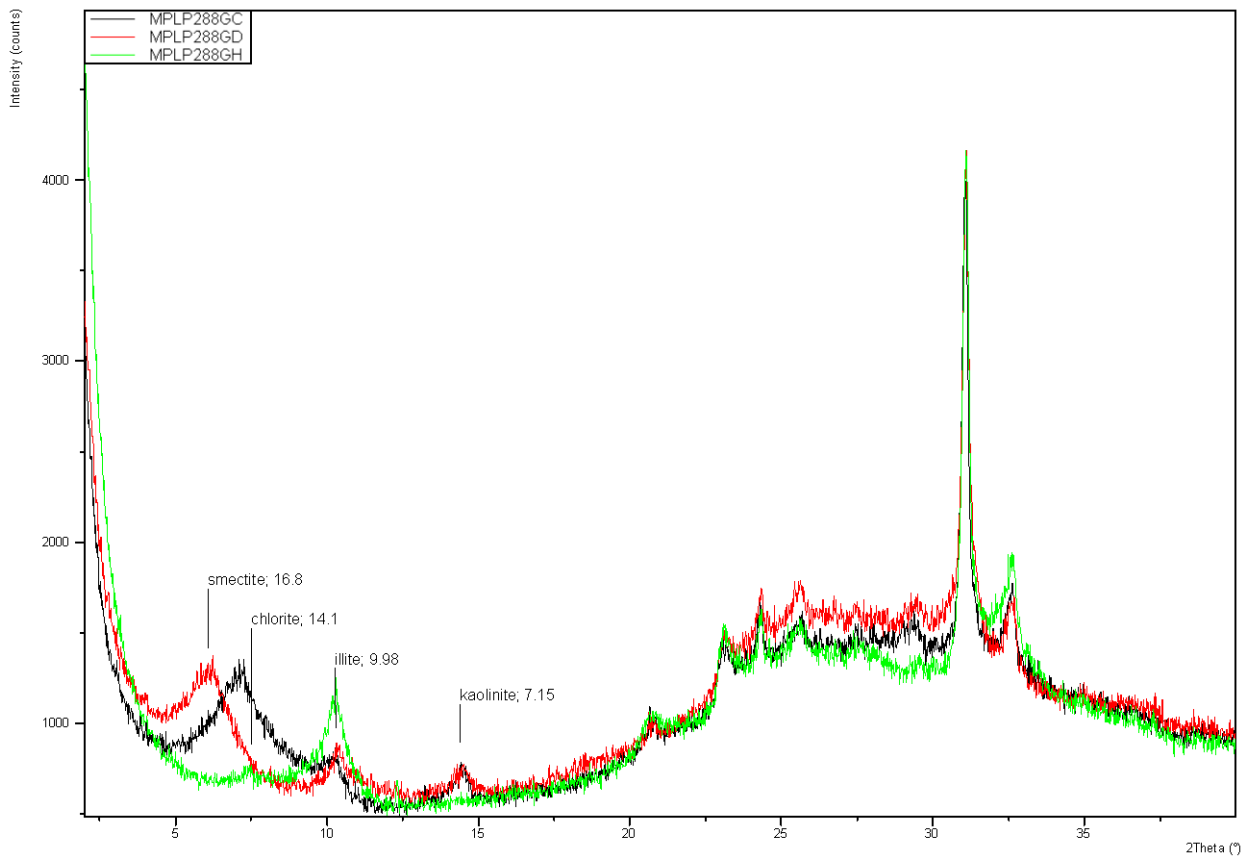
The upper figure on each page shows the sample diffraction trace. The lower figure on each page shows stick pattern data for the extracted sample peaks (orange) and the identified mineral standard data.

For the  $<2 \mu\text{m}$  traces, black trace (air-dry), red trace (glycol-solvated), green trace (heated  $550^{\circ}\text{C}/2$  hours). Only the most intense/diagnostic peak of each identified mineral is labelled with its corresponding  $d(\text{\AA})$  spacing.

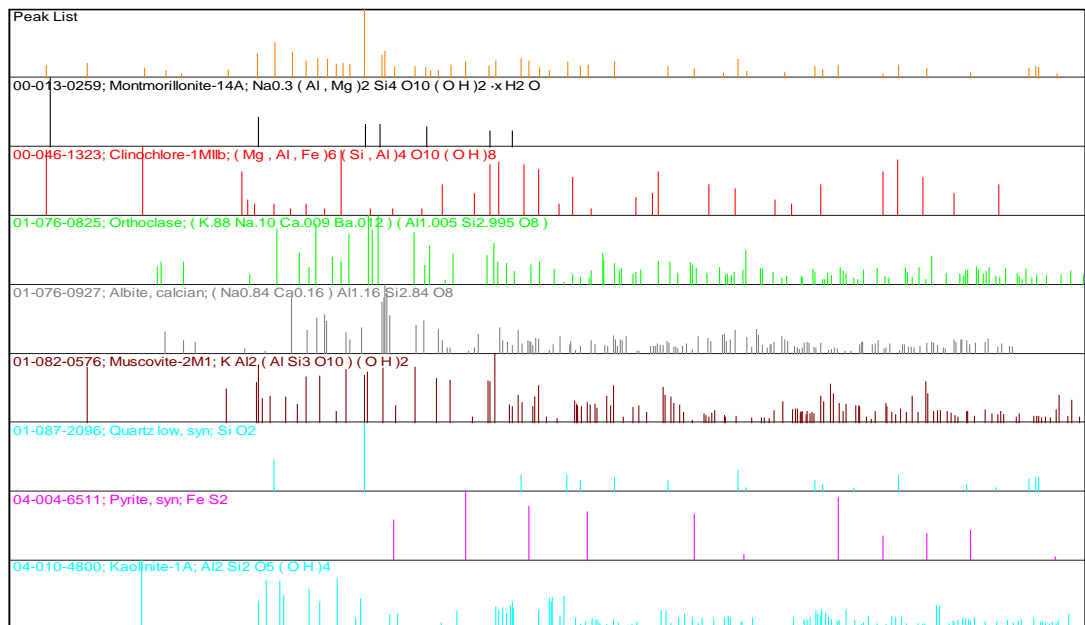
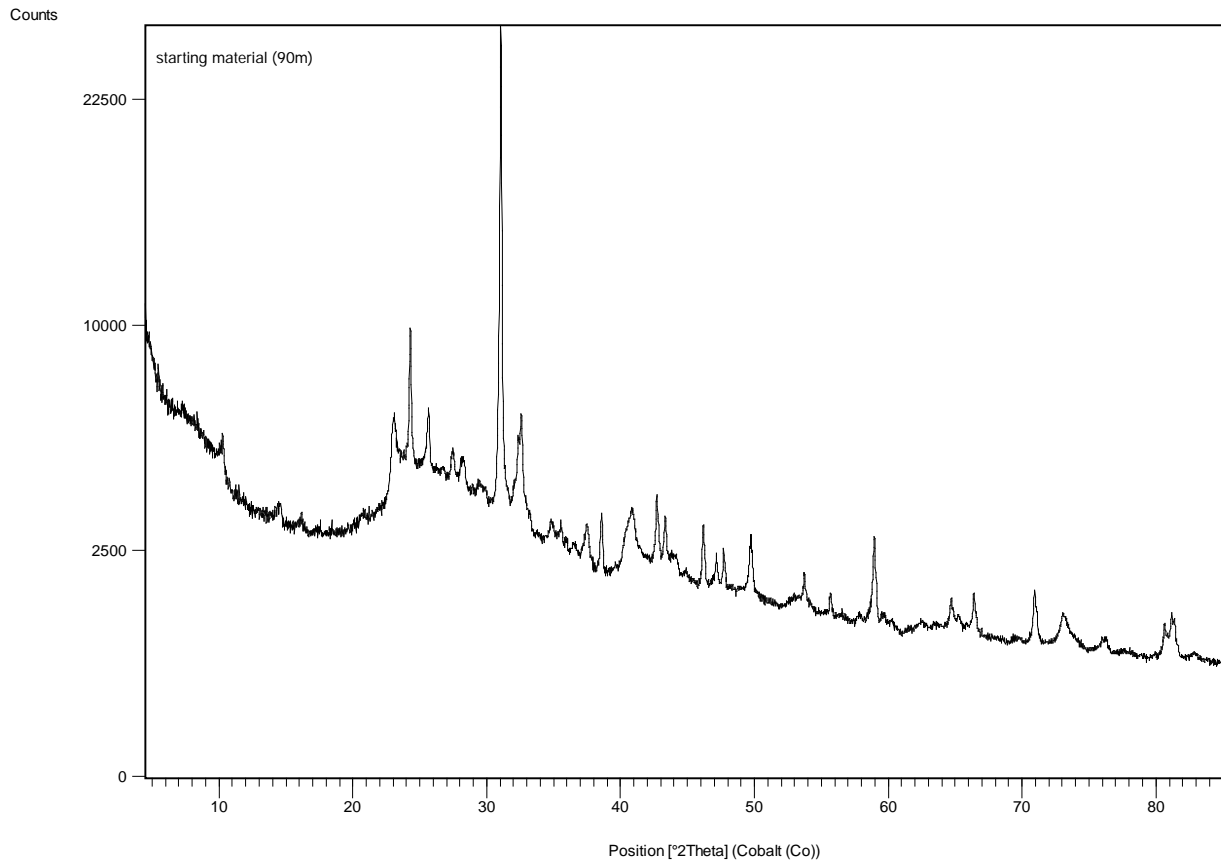
### Starting material (40m) - whole-rock



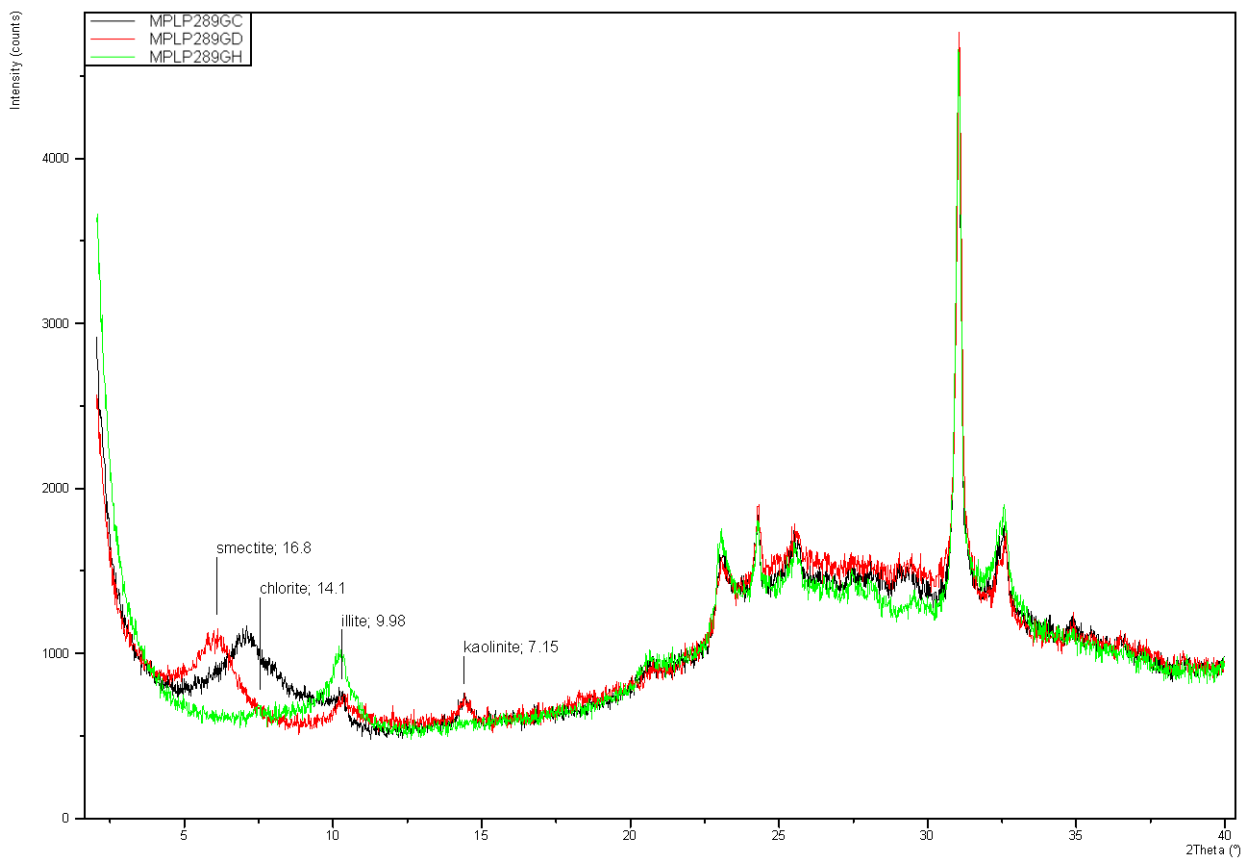
### Starting material (40m) - <2 μm clay fraction



### Starting material (90m) - whole-rock



### Starting material (90m) - <2 μm clay fraction



## References

British Geological Survey holds most of the references listed below, and copies may be obtained via the library service subject to copyright legislation (contact libuser@bgs.ac.uk for details). The library catalogue is available at: <http://geolib.bgs.ac.uk>.

BATEMAN, K., COOMBS, P., LACINSKA, A., MILODOWSKI, A. E., WAGNER, D. AND WEST, J. M. 2009 MICROBIOLOGICAL INFLUENCES ON THE GEOLOGICAL DISPOSAL OF RADIOACTIVE WASTE – DATE PRODUCTION FOR HORONOBE. BRITISH GEOLOGICAL SURVEY REPORT CR/09/25.

BEVERIDGE, T. J., MAKIN, S. A. AND KADURUGAMUWA, J. L. & LI, Z. (1997) Interactions between biofilms and the environment. *FEMS Microbiology Reviews* **20**, 291-303

CHAPELLE, F.H. (2000) *Ground-water microbiology and geochemistry*: New York, John Wiley and Sons, 468 pp

COOMBS, P., WEST, J. M., WAGNER, D., TURNER, G., NOY, D. J., MILODOWSKI, A. E., LACINSKA, A., HARRISON, H. AND BATEMAN, K. (2008) Influence of biofilms on transport of fluids in subsurface granitic environments – Some mineralogical and petrographical observations of materials from column experiments. *Mineralogical Magazine* **72(1)** 393-397

EHRlich, H. L. (1999) Microbes as geologic agents: their role in mineral formation. *Geomicrobiology Journal* **16**, 135-153

GOLDSTEIN, J.I., NEWBURY, D.E., ECHLIN, P., JOY, D.C., FIORI, C. AND LIFSHIN, E. 1981. Scanning Electron Microscopy and X-Ray Microanalysis. Plenum Press, New York.

HALLBECK, L. AND PEDERSEN, K. (2008) Characterisation of microbial processes in deep aquifers of the Fennoscandian Shield. *Applied Geochemistry*, **23**, 1796-1819.

HAMA, K., BATEMAN, K., COOMBS, P. HARDS, V.L., MILODOWSKI, A.E., WEST, J.M., WETTON, P.D., YOSHIDA, H., AOKI, K., (2001) Influence of bacteria on rock-water interaction and clay mineral formation in subsurface granitic environments. *Clay Minerals* **36**, 599-613.

HOBBIE, J. E., DALEY, R. J. AND JASPER, S. (1977) Use of nucleopore filters for counting bacteria by fluorescent microscopy. *Applied and Environmental Microbiology* **33**, 1225-1228.

JASS, J. AND LAPPIN-SCOTT, H M, 1992. PRACTICAL COURSE ON BIOFILM FORMATION USING THE MODIFIED ROBBINS DEVICE UNIVERSITY OF EXETER.

KONHAUSER, K. O., FISHER, Q. J., FYFE, W.S., LONGSTAFF, F. J. & POWELL, M. A. (1998) Authigenic mineralisation and detrital clay binding by freshwater biofilms: The Brahmani River, India. *Geomicrobiology Journal* **15**, 209-222.

KONHAUSER, K. O. (2007) *Introduction to Geomicrobiology*. Blackwell Science Ltd, Malden MA. USA. 425 pp

MILODOWSKI, A. E., WEST, J. M., PEARCE, J. M., HYSLOP, E. K., BASHAM, I. R. AND HOOKER, P. J. (1990) Uranium-mineralised microorganisms associated with uraniferous hydrocarbons in southwest Scotland. *Nature* **347**, 465-467.

PARKHURST, D.L. AND APPELO, C.A.J., 1999. USER'S GUIDE TO PHREEQC (VERSION 2) - A COMPUTER PROGRAM FOR SPECIATION, REACTION-PATH, 1D-TRANSPORT, AND INVERSE GEOCHEMICAL CALCULATIONS. US GEOL. SURV. WATER RESOUR. INV. REP. 99-4259, 312p

POLSON, E. J., BUCKMAN, J. O., BOWEN, D. G., TODD, A. C., GOW, M. M. AND CUTHBERT, S. J. (2010) An environmental scanning electron microscope investigation into the effect of biofilm on the wettability of quartz. *Society of Petroleum Engineers Journal* **15**, 223-227

SHOCK, E. L. (2009) Minerals and energy sources for microorganisms. *Economic Geology* **104**, 1235-1248.

SOUTHAM, G., AND SAUNDERS, J. A. (2005) The geomicrobiology of ore deposits. *Economic Geology* **100**, 1067-1084.

STROES-GASCOYNE, S. AND WEST, J. M. (1996) An overview of microbial research related to high-level nuclear waste disposal with emphasis on the Canadian concept for the disposal of nuclear fuel waste. *Canadian Journal of Microbiology* **42**, 349-366.

STROES-GASCOYNE, S., SCHIPPERS, A., SCHWYN, B., POULAIN, S., SERGEANT, C., SIMANOFF, M., LE MARREC, C., ALTMANN, S., NAGAOKA, T., MAUCLAIRE, L., MCKENZIE, J., DAUMAS, S., VINSOT, A., BEAUCAIRE, C. AND MATRAY, S-M. (2007) Microbial community analysis of Opalinus Clay drill core samples from the Mont Terri Underground Research Laboratory, Switzerland. *Geomicrobiology Journal* **24**, 1-17

SNYDER, R.L. AND BISH, D.L. (1989) Quantitative analysis. In: Bish, D.L., Post, J.E. (Eds), Mineralogical Society of America, USA. *Modern Powder Diffraction, Reviews in Mineralogy* **20**, 101-144.

TOCHIGI, Y., YOSHIKAWA, H. AND YUI, M. 2007. Modelling studies on microbial effects on groundwater chemistry. Scientific Basis for Nuclear Waste Management XXX 985, 575-580.

TUCK, V. A., EDYVEAN, R. G.J., WEST, J. M., BATEMAN, K., COOMBS, P., MILODOWSKI, A. E. AND MCKERVEY, J. A. (2006) Biologically induced clay formation in subsurface granitic environments. *Journal of Geochemical Exploration* **90**, 123-133